2012

Combining electrospun polydioxanone scaffolds, Schwann cells, and Matrigel to improve functional recovery after a complete spinal cord transection in rats

Ashok Kannan
Virginia Commonwealth University

Combining Electrospun Polydioxanone Scaffolds, Schwann Cells, and Matrigel to Improve Functional Recovery after a Complete Spinal Cord Transection in Rats

A thesis submitted in partial fulfillment of the requirements for a Master of Science degree in Anatomy and Neurobiology at Virginia Commonwealth University

by:

Ashok Kannan
B.A., Spanish Literature, North Carolina State University at Raleigh, 2010
B.A., Psychology, North Carolina State University at Raleigh, 2010

Director and Advisor:
Raymond J. Colello, D.Phil
Associate Professor, Department of Anatomy and Neurobiology

Virginia Commonwealth University
Richmond, Virginia
May 2012

Acknowledgements

My supreme gratitude and appreciation is first expressed towards my advisor and this project's principal investigator Dr. Raymond Colello, D. Phil. Dr. Colello's enthusiasm for spinal cord injury research and desire to cultivate boundless analytical thinking in the minds of his students is impressive. I have learned a great deal by simply listening to and watching how he approaches obstacles and it has been a true pleasure to be his student.

I would like to secondly thank my committee members, Dr. David Simpson, Dr. Jeffrey Dupree, and Dr. Dong Sun, in no particular order, for their time and effort. Their input shaped my project and my approach to it from the beginning, and thus this work would truly not have been possible without them.

I would additionally like to thank Dr. Shekhar Jha, Damien Brown, Matt Baer, and an unnamed peer for their work on this project and for their constant support. They, better than anyone, know the extent of the effort that was coordinated to afford everything that this project required.

TABLE OF CONTENTS

LIST OF FIGURES

LIST OF ABBREVIATIONS

2D	two-dimensional
3D	three-dimensional
CNS	central nervous system
SCI	spinal cord injury
SC	Schwann cell
PI3K	phosphatidylinositol-3-kinase
IL	interleukin
TNF	tumor necrosis factor
FGF	fibroblast growth factor
NGF	nerve growth factor
NT-3	neurotrophin-3
OD	oligodendrocyte
MAG	myelin-associated glycoprotein
Omgp	oligodendrocyte-myelin glycoprotein
NgR	Nogo receptor
OPC	oligodendrocyte precursor cell
GFAP	glial fibrillary acidic protein
CSPG	chondroitin-sulfated proteoglycan
GAG	glysoaminoglycan
PNS	peripheral nervous system
BDNF	brain-derived neurotrophic factor
GDNF	glial-cell derived neurotrophic factor

CNTF	ciliary neurotrophic factor
ECM	extracellular matrix
HGF	hepatocyte growth factor
TGF	transforming growth factor
chABC	chondroitinase ABC
NTPH/NTP	neurotrophin/neurotropin
IGF	insulin-like growth factor
hMSC	human bone marrow-derived mesenchymal cells
VEGF	vascular endothelial growth factor
PCL	poly-ε-caprolactone
PLGA	polylactic-co-glycolic acid
PLA	poly-L-lactic acid
HA	hyaluronic acid
OPF	oligo polyethylene glycol fumarate
T8	eighth thoracic vertebtra
PDS	polydioxanone suture
HFP	1,1,1,3,3,3-Hexafluoro-2-propanol
HFIP	hexafluoroisopropanol
SD	standard deviation
TBS	tris-buffered saline
SC bridge (both sides)	scaffold + Matrigel™ + SCs on both sides
rostrally-facing SC bridge	scaffold + Matrigel™ + SCs on one side (implanted into animal with cellularized side facing rostrally)

caudally-facing SC bridge	scaffold + Matrigel™ + SCs on one side (implanted into animal with cellularized side facing caudally)
Matrigel™-only bridge	scaffold + Matrigel™ + control treatment (SC medium)
control bridge	scaffold + control treatment (SC medium)
HBSS	Hank's balanced salt solution
dura	dura mater
BBB	Basso-Beattie-Bresnahan
IC	intracellular
BSA	bovine serum albumin
PBS	phosphate-buffered saline
ANOVA	analysis of variance
T	time
SEM	standard error of mean
MHC	myosin heavy-chain
hESC	human embryonic stem cell
Tukey's test	Tukey's multiple comparison test

ABSTRACT

COMBINING ELECTROSPUN POLYDIOXANONE SCAFFOLDS, SCHWANN CELLS, AND MATRIGEL TO IMPROVE FUNCTIONAL RECOVERY AFTER A COMPLETE SPINAL CORD TRANSECTION IN RATS

Ashok Kannan, Master of Science

A thesis submitted in partial fulfillment of the requirements for a Master of Science degree in Anatomy and Neurobiology at Virginia Commonwealth University

Virginia Commonwealth University, 2011

Raymond J. Colello, D.Phil., Associate Professor, Department of Anatomy and Neurobiology

Spinal cord injury (SCI) has presented itself as a multifaceted pathology that is largely inhibitory to regeneration, and therefore to functional recovery, even though spinal cord neurons have been found to be innately regenerative. Thus, having identified the key players in the inhibition of this innate regeneration, SCI researchers have focused on two major types of approaches: (1) blocking inhibitory cues and (2) promoting innate regeneration. Schwann cells (SCs) have long been shown to promote and enhance functional recovery after SCI through providing supplemental myelination and trophic and tropic factors to regenerating axons, though singular approaches rarely address the complex SCI pathology. Guidance channels and scaffolds have been shown to provide physical support and directional cues to regeneration axons. Therefore, a combinatorial approach in which SCs migrate into and throughout a guidance scaffold would be an ideal research focus for treating SCI. However, cell migration into guidance scaffolds has been shown to be problematic. This study attempts to assess and improve two- and three-dimensional SC migration on electrospun scaffolds. Additionally, we evaluate the ability of SCs, seeded on Matrigel-coated electrospun scaffolds, to improve functional recovery in rats with completely transected spinal cords.

INTRODUCTION

Originally viewed as inflexible to and unsupportive of regeneration, the adult central nervous system's reputation has been upended in the past century, lending itself to a host of clinically-significant alterations. Since this transformation, spinal cord injury treatment and the approach to improving it has progressed aggressively. Following findings that the central nervous system (CNS) neurons can regenerate (Aguayo, 1981) and that local axonal sprouting was a probable mechanism for regeneration (Selzer, 1978; Raisman, 1978), spinal cord injury (SCI) research began to focus on altering the injury environment to facilitate this axonal regeneration. However, these regeneration attempts were frequently deterred by the multitude of inhibitory cell types and molecules present at the SCI site (Fawcett and Asher, 1999). Promising strategies have thus fallen under two categories: (1) Those that block cues that inhibit regeneration and (2) those that provide or enhance growth-promoting cues that allow regeneration to overcome inhibitory cues (Fouad et al., 2005). Though many desirable endpoints of CNS repair, such as full, functional control of locomotion and of micturition, have not been reached consistently in humans or in animal models, CNS repair strategies after SCI have shown significant improvement and potential. The transplantation of Schwann cells (SCs) into the SCI site to aid recovery has been established as an effective strategy, comprising elements that block regeneration inhibition and strongly enhance axonal health and regeneration (Duncan, Aguayo, Bunge, Wood, 1981; Bunge, 2008). However, the inability of SCs to address all SCI deficiencies has led to the call for combination strategies. Recently, the use of electrospinning to bioengineer scaffolds for the guidance and support of both implanted and native cells has been shown to be used, alone and in combination, in central nerve regeneration attempts (Tabesh et al., 2009). This paper will briefly overview the cellular response with attention to the ability of each majorly

involved cell type to aid SCI recovery, review the strengths and weaknesses of the most popularly published SCI recovery strategies, present Schwann cells and bioengineered axonal guidance scaffolds as promising strategies to attenuate this inhibition, and review the results of a project that evaluated their combination as a way to improve SCI recovery.

Chapter 1:

The Cellular Response to SCI

A progressive phenomenon, SCI pathophysiology arguably comprises different stages. After insult, the CNS incurs primary, secondary, and tertiary lesions. Primary lesions, such as compressed or cut axons, are normally direct effects of the damaging agent (ex. physical impact or toxin). These injurious physiological changes usually lead to secondary lesions, including ischemia, axonal degradation, anoxia, and free radical formation, which then cause tertiary lesions, including immune cell recruitment, glial scar formation, and neuronal and glial cell death (Du et al., 2011; Onifer et al., 2007; Zhilai et al., 2011; Zong et al., 2011).

Upon insult, various cell types endogenous to the CNS undergo major modifications, while cell types exogenous to the CNS migrate into the injury site milieu. Endogenous cell types that undergo major alterations include astrocytes, oligodendrocytes, microglia/macrophages, oligodendrocyte precursors, and multipotential progenitor cells. Cells that migrate into the CNS after injury include Schwann cells (SCs), meningeal cells, and monocytes/macrophages. This section will briefly summarize actions of the some of these cell types in the context of regeneration and repair, focusing finally on SCs and why they are arguably the most conducive to repair and regeneration.

Neurons

Following the destruction of axonal segments, both the proximal and distal ends degenerate. The distal ends of affected neurons usually undergo complete structural disintegration and chemical degradation in which the axolemma beads and swells and microtubules, neurofilaments and other cytoskeleton components undergo granular disintegration

(Vargas and Barres, 2007); this is termed Wallerian degeneration (Lavdas et al., 2008).Complementary to this process, central chromatolysis, which was first described by the disintegration of Nissl substance and has come to define the general degenerative response after axonal injury, occurs in the proximal end of affected neurons (Tellez et al., 1987). The corresponding myelin sheath, whose integrity depends both on the health of the providing oligodendrocyte and on the structure of the axon it is enveloping, undergoes a systematic degradation. This degenerative response is driven partially by the cellular release of an excess of excitatory amino acids and consequent prolonged receptor activation that triggers an excessive Ca^{2+} influx and Ca^{2+}-invoked activation of proteolytic and degradative enzymes, particularly cysteine proteases calpain and cathepsin (Yamashima, 2004). These enzymes breakdown cytoskeletal proteins and instigate reactive oxygen species release, leading to membrane damage and chemokine and cytokine production as well as other intracellular (ex. mitochondrial) dysfunctions (Bunge, 2008; Sauerbeck et al., 2011).

Primary and secondary cell necrosis is regulated, at least in part, by phosphatidylinositol-3-kinase (PI3K)/Akt signaling. Though activation of this pathway contributes to the prevention of cell death and to the enhancement of growth- and proliferation-associated cellular processes, Akt phosphorylation at and around the injury epicenter is abated after SCI, altering and rendering this pathway dysfunctional. This enervation contributes to the widespread necrosis at and around the injury site (Walker et al., 2012).

Macrophages, Microglia, and Monocytes

The non-neuronal cellular response to SCI recovery, however, is arguably a more effective target for improving recovery. The immune system's cells, such as neutrophils and macrophages/monocytes/microglia, invade the injury site as part of an acute inflammatory

response. These cells produce proteolytic and oxidative enzymes, such as matrix metalloproteinases, proinflammatory cytokines, and interleukins (ex. interleukin (IL)-1β, tumor necrosis factor (TNF)-α, IL-1, and IL-10), triggering a more comprehensive immune response (Nakajima et al., 2012; Wright et al., 2011; Zong et al., 2011). This response by the immune system includes processes that both promote and inhibit CNS regeneration and repair. Proteolytic and oxidative enzymes from immune cells can cause increased cavitation and cyst formation at the lesion site, exacerbating neurological dysfunction. However, macrophages have been found to phagocytose myelin debris in the injured spinal cord that could otherwise prevent axonal regeneration and also produce protective cytokines such as fibroblast growth factor (FGF), nerve growth factor (NGF), and neurotrophin-3 (NT-3), all of which promote neuronal regeneration (Nakajima et al., 2012; Shechter et al., 2011). The use of a cell type that can express these protective and growth-promoting factors while not producing the harmful factors that are expressed by the immune cells would be an ideal approach to improving recovery after SCI.

Oligodendrocytes and Oligodendrocyte Precursor Cells

Alongside the immune cell response is a momentous glial cell response. Oligodendrocytes (ODs) debilitated by the physical insult or by secondary lesions become less effective as myelinating agents, further impairing axonal action potential conduction. Damaged myelin sheaths, either due to the trauma itself or to OD death, break up into myelin debris chunks that are slowly collected by microglia and macrophages (Fawcett and Asher, 1999). Oligodendrocytes additionally express a set of compounds, including myelin-associated glycoprotein (MAG), Nogo-A, and oligodendrocyte-myelin glycoprotein (Omgp), that inhibit axonal regrowth. MAG, a potent inhibitor of neurite outgrowth, acts through the Nogo-66 receptor (NgR) complex. Nogo-A's inhibitory activity is mediated through its interaction with

NgR and other known and unknown Nogo-A receptors in the CNS, while Omgp's inhibitory activity is dependent on the fidelity of the NgR complex alone, as cleavage of NgR renders axons insensitive to Omgp-induced growth inhibition (Gang et al., 2010; Wright et al., 2011; Zhilai et al., 2011; etc.).

After widespread OD necrosis and apoptosis, the replacement of myelin-producing cells becomes vital to functional recovery. Oligodendrocyte precursor cells (OPCs), which are present largely in white matter of the adult CNS, though they were first found in the optic nerve, proliferate and migrate to CNS injury site to remyelinate unmyelinated axons. While some OPCs mature into oligodendrocytes, the maturation of many OPCs is halted by either the inhibitory environment of the injury site or the lack of growth factors and molecular cues that promote full remyelination. Thus, remyelination by OPCs rarely reaches completion (Mekhail et al., 2012; Wu et al., 2011). Finding a more sustainable mode of remyelination is vital to improving functional recovery after SCI.

Astrocytes

A glial-cell directive, in which astrocytes become reactive and start expressing high levels of glial fibrillary acidic protein (GFAP), forms a scar around the fluid-filled cystic cavity that constitutes the lesion site. The newly formed scar encases the lesioned CNS site in a manner that effectively quarantines any exacerbating processes (ex. the destruction of healthy neural cells by reactive compounds and activated immune cells) while simultaneously preventing any extra-cystic elements (ex. regenerating axons) from interacting with the cyst. In fact, injured, regrowing axons terminate dystrophically at the outer margins of the lesion, indicating thwarted axonal growth (Fortun et al., 2009; Afshari et al., 2010; Deng et al., 2011). The deterrent nature of the glial scar is especially obstructive to axonal regeneration and regrowth. Though they help

to repair the blood-brain barrier and help to hault injury propagation, glial-scar astrocytes express a host of inhibitory compounds, of which the most significant are chondroitin-sulfated proteoglycans (CSPGs). CSPGs consist of a protein core to which glycosaminoglycan (GAG) side-chains are attached. These GAG side-chains have been suggested to be the basis of the inhibitory effect of CSPGs. It has also been shown that chondroitinase ABC, which cleaves these GAG side-chains, reduces CSPG-mediated inhibition of axonal regeneration in vivo and of neurite formation in vitro (Gang et al., 2010; Wright et al., 2011; etc.). The inhibition of the astrocytic obstruction of axonal regeneration is key for any SCI recovery improvement strategy.

Schwann Cells

Upon spinal cord injury, endogenous SCs invade the injured spinal cord milieu from the area of the spinal cord-nerve root junction in the proximal peripheral nervous system (PNS) to associate with regenerating axons (Blakemore, 1975; Blakemore, 1977; Duncan et al., 1988; Harrison, 1985). Each SC wraps itself around an axonal section, which constitutes a section of the myelin sheath around an axon, thus the myelin sheath around the axon of one neuron comprises numerous SCs. Each SC that has wrapped itself around one section of the axon localizes a certain distance from adjacent myelinating SCs, leaving spaces between myelinated sections of the axon constituting the Nodes of Ranvier. The newly created myelin sheath is surrounded by a unique basal lamina of mucopolysaccharides, which are secreted from the SCs (Fortun et al., 2009; Lavdas et al., 2008).

In addition to re-myelination, SCs produce and release a volley of neurotrophic and growth factors, including NGF, brain-derived neurotrophic factor (BDGF), NT-3, FGF, glial-cell derived neurotrophic factor (GDNF), and ciliary neurotrophic factor (CNTF). They additionally release various cell adhesion molecules (ex. integrins, N-cadherin, N-CAM, L1, and contactin)

and extracellular matrix proteins (ex. laminin, fibronectin, and collagens), additionally supporting regrowing axons.

However, the endogenous SC response in SCI is limited and frequently ineffective in improving functional recovery. This is due, in part, to the limited migration of SCs that have invaded the CNS white and grey matter, even though they are typically highly migratory. Though restricted intra-CNS injury site migration of SCs may be attributed to reactive astrocytes, astrocytes have also been found to be stimulatory in SC migration when SCs and astrocytes are co-implanted, thus the reason for this impaired migration is still unknown (Afshari et al., 2010; Blakemore, 1975; Evercooren et al., 1997).

SCs are arguably the most conducive SCI-responsive cell-type for functional recovery. SCs produce the protective and growth-promoting factors produced by macrophages and microglia, but do not producing the pro-inflammatory cytokines released by these cells. Additionally, when compared to oligodendrocytes, SCs can survive for long periods of time in the spinal cord lesion environment and are less susceptible to the necrosis/apoptosis promoting factors of the injury site. Also, SCs are less susceptible to autoimmune responses, such as in multiple sclerosis, than oligodendrocytes. In contrast to astrocytes, SCs do not produce significant amounts of compounds inhibitory to axonal regeneration. Also, astrocytes, unlike SCs, lack myelinating properties, making SCs the more desirable therapeutic candidate (Bunge, 2002; Fawcett and Asher, 1999; Takami et al., 2002)

Despite their many advantages, SCs remain an imperfect method by which to improve functional recovery after SCI. Possibly the most notable drawback is their limited ability to migrate away from the implantation or injection site (Afshari et al., 2010; Andrews & Stelzner, 2007). This weakness is due, in part, to the tendency of SCs to spatially segregate from host

astrocytes, which inundate the CNS injury site. In fact growing astrocytes and SCs have been found to form stern boundaries upon contact *in vitro* and *in vivo*, though the full implications of this behavior have yet to be explored. Other factors that may contribute to the restricted Schwann cell migration include proteoglycans, heparin/FGF signaling, ephrin-eph signaling, and N-cadherins (Afshari and Fawcett, 2012; Afshari et al., 2010). To address the problem of limited SC migration after implantation or injection, many groups have focused on combinatorial strategies in which SCs are coupled with growth-promoting, guidance-providing substrates and scaffolds to which they are allowed to attach and infiltrate prior to being implanted into animals. In this way, SCs can be initially provided throughout the injury site and, even after being implanted into the injury site, can use the guiding nature of the scaffold to migrate more effectively (Fouad et al., 2005). Experiments presented in this paper reflect a pursuit of this concept, in an attempt to optimize the use of SCs, which present themselves as a promising strategy in SCI recovery, seeded on nanofiber scaffolds fashioned by electrospinning.

Chapter 2:

SCI Repair Strategies

Despite a rapid evolution of *in vitro* and *in vivo* research approaches to improve SCI repair, functional restoration and recovery successes have been limited (Joo et al., 2012). As mentioned, singular therapies have traditionally fallen under one of two classifications: (1) Those that block cues that inhibit regeneration and (2) those that provide or enhance growth-promoting cues. Though, many combinatorial and singular therapies employ both approaches. Specific goals for therapies addressing spinal cord injury include halting the spread of secondary tissue damage, curbing inflammation, reducing glial scar formation, neutralizing inhibitory factors, stimulating nerve fibers to regrow, nourishing surviving nerve cells, promoting physical fiber growth across the injury area, directionally guiding physical growth, and enabling connection establishment (Bunge, 2008). This section will overview strengths and limitations of some of the more popularly published therapy strategies, establish exogenous SC implants and the bioengineered scaffold implants as relatively promising therapies for SCI recovery separately, and then present an argument for their combination.

Physical Rehabilitation

Handicapped or non-existent standing and stepping patterns after a severe SCI have been shown to be resultant of a depressed state of spinal neuronal networks. However, neuronal circuits that experience repeated sensory and motor pathway activation can be reestablished and reinforced. This activity-dependent plasticity underlies the mechanism by which many rehabilitation studies achieve recovery. However, daily task-specific training improves the function of only the trained task (i.e. cats that had been intensively trained to stand exhibited an

improved capacity to stand, but had no apparent stepping improvements) (Musienko et al., 2011). Motor and sensorimotor recovery from exercise after SCI have been observed using behavioral and anatomical tests. Molecular quantification, such as measuring changes in levels of proteins such as BDNF, show results after just five days of exercise (Sandrow-Feinberg et al., 2009). Post-SCI exercise has also been found to stabilize lumbar motoneuron rhythmic firing patterns, increase levels of neurotrophic factors in the spinal cord, and reduce inflammation (Liu et al., 2012). Physical rehabilitation has failed to produce prominent long-term effects, resulting in its frequent combination with other strategies.

Glial Scar Digestion and Inhibitory Factor Neutralization

Following secondary and tertiary tissue damage after SCI, an intrinsic inflammatory response ensues, contributing to cavitation and cyst formation at the lesion center and resulting in a glial scarring that is inhibitory to axonal regrowth and regeneration. Attempts to reduce or inhibit components of this glial scar have produced promising results. Cellular approaches include the acute injection of mesenchymal stem cells into an SCI site has been used to modify the inflammatory response to SCI to subsequently reduce scar tissue and cavity formation, thus creating a more permissive environment for axonal regeneration (Nakajima et al., 2012). This approach, though, addresses only the glial scar's inhibition of regeneration; the remyelination of unmyelinated axons, the provision of neurotrophic/neurotropic factors to aid regeneration, and the establishment of an extracellular matrix (ECM) that is conducive to regeneration and guidance are all not addressed.

Acellular strategies, have been shown to successfully suppress glial scar formation after CNS injury through mechanisms such as the attenuation of astrocytic activation and inhibitory

factor production, hence allowing axonal growth into the lesion cavity. The administration of hepatocyte growth factor (HGF), for example, has been found to reduce inhibitory CSPG expression and transforming growth factor (TGF)β levels as well as the activation of astrocytes *in vitro* and *in vivo* (Jeong et al., 2012). CSPGs, one of many ECM molecules that the glial scar comprises, are especially inhibitory to axonal growth and glial progenitor cell process outgrowth *in vitro* and *in vivo*, and thus chondroitinase ABC (chABC) has been used to effectively remove CSPG GAG chains, thus attenuating CSPG inhibitory activity (Bradbury et al., 2002; Siebert & Osterhout, 2011). However, the administration of factors that attenuate the inhibition of axonal regeneration addresses only one facet of SCI and tend to have a short therapeutic windows *in vivo*, since they may be degraded.

Electrical Stimulation

Altered signal transmission in surviving and regenerating axons after SCI, which underlies various components of SCI pathology, can be attributed to conduction deficits in response to increased action potential thresholds (Hunanyan et al., 2012). Thus, electrical stimulation can be used to induce action potentials by overcoming high thresholds. Tonic epidural electrical stimulation has been shown to restore hindlimb movements in otherwise paralyzed rats, and it has thus been coupled with physical rehabilitation strategies to improve recovery in various animal models (Courtine et al., 2011). Additionally, electric fields have been successfully implicated in improving cell (astrocyte) migration and enhancing cell (oligodendrocyte) viability in CNS injury models (Gary et al., 2012; Li et al., 2010). Though focal electrical stimulation may be able to change many aspects of cell behavior, the more clinically-relevant stimulation of various cells or tissues may alter important physiological

micro- and macroscopic electrostatic forces, thus possibly altering important homeostatic balances.

Neurotrophic/Neurotropic Factor Delivery

The topical administration of neurotrophins/neurotropins (NTPHs/NTPs), including NGF, BDNF, GDNF, and insulin-like growth factor (IGF-1) have been shown to improve functional recovery after SCI. BDNF or IGF-1 administered onto the SCI site induces neuroprotection, while the topical administration of BDNF with IGF-1 and GDNF improved motor function just 90 min after SCI (Sharma & Sharma, 2012). Topical administration, however, does not afford the spatial and temporal control of NTPH/NTP release offered by cells or degradable polymer carriers. Thus, a host of different vehicles, including cells and polymer encasings (ex. beads), have been used to deliver neurotrophic/neurotropic and growth factors in *in vivo* and *in vitro* SCI models. When administered locally, these extrinsic signaling cues have been shown to significantly improve axonal survival and regrowth/regeneration, and subsequently functional recovery (Krick et al., 2011; Sharma & Sharma, 2012). The therapeutic window duration of this method is a direct function of properties of the biomaterial used to fashion the encasing, thus limiting NTPH/NTP release to parameters set by these material properties. Whereas polymer beads may have limited molecular release durations, cells that are implanted into injury environments *in vivo* may be able to survive, replicate, and thrive. Thus cells that innately or that have been engineered to produce desired NTPHs/NTPs are attractive administration alternatives. The delivery of growth and neurotrophic/neurotropic factors via cells has produced promising results. Many cellular strategies to SCI repair and regeneration have focused on using transplanted SCs as a source of neurotrophic/neurotropic factors (Bunge, 2008). In fact, human

bone marrow-derived mesenchymal stem cells (hMSCs) induced to adopt SC characteristics have been found to express SC-specific proteins, to adopt an SC-like morphology, and to secrete higher concentrations of several growth factors, such as vascular endothelial growth factor (VEGF) and HGF, usually secreted by normal hMSCs. Thus, like SCs, these altered hMSCs produce a host of neurotrophic and neurotropic factors (Park et al., 2010).

Re-myelination

Two of the most popularly researched molecular approaches to post-SCI myelin repair are (1) preserving existing oligodendrocytes and (2) increasing the presence of myelinating agents, such as oligodendrocyte precursor cells, olfactory ensheathing cells, and Schwann cells (Mekhail et al., 2012; Tharion et al., 2011).

The preservation of existing myelinating cells after SCI, though relatively unimodal, has opened promising avenues of pursuit. The rescue of apoptotic oligodendrocytes, reduction in myelin loss, and subsequent improvement in functional recovery are all seen after the administration of gastric hormone ghrelin, which is known to stimulate growth hormone release from the hypothalamus and pituitary gland (Lee et al., 2010). Successful attempts to preserve existing myelinating cells after SCI also include the use of topiramate, a 2-amino-3-(5-methyl-3-oxo-1,2- oxazol-4-yl)propanoic acid (AMPA)-specific glutamate receptor agonist that is FDA-approved to treat CNS disorders, and leukemia inhibitory factor, which acts through JAK/STAT and Akt signaling (Azari et al., 2006; Butzkueven et al., 2006; Gensel et al., 2012).

To supplement the preservation of surviving oligodendrocytes, a faction of research studying remyelination after nerve injury research has focused on adding myelinating agents, such as oligodendrocytes (ODs), oligodendrocyte precursor cells (OPCs), olfactory ensheathing

cells (OECs), and Schwann cells SCs). Increasing oligodendrocyte number at and around the injury site has been shown to improve action potential conduction in initially amyelinated axons (Almad et al., 2011; Utzschneider et al., 1994). Strong evidence has been shown to support that the transplantation of OPCs (Keirstead et al., 2005; Wu et al., 2011), OECs (Novikova et al., 2011; Tharion et al., 2011) and SCs (Bunge, 2008; Chen et al., 2002; Deng et al., 2011) improve remyelination in the injured cord and enhance functional recovery after SCI. The use of non-OD cell types resulted from the hostility to ODs displayed by the post-SCI environment. Of the myelinating cells, SCs seem to be the best choice for addressing the multifaceted impact of SCI. Compared to SCs, OECs have been shown to be less viable and to provide less myelination post-implantation. Likewise, OPCs, though viable in the hostile post-SCI environment and an active remyelinating agent of denuded axons, produce myelin that is thinner, has shorter internode segments, and irregular ratios of axon radius to axon plus surrounding myelin radius. Though myelination by SCs after SCI has resulted in imperfect action potential conduction, many groups cite ease of culturing and harvesting large numbers of SCs, as well as potential ease of clinical translation since SCs could be taken from patients' peripheral nerves, as reasons for pursuing SCs over OECs and OPCs (Bunge, 2008; Oudega, 2007; Pearse et al., 2007).

Axonal Guidance Support

Though biochemical approaches, such as supplemental myelination and trophic/tropic factors, to improve SCI recovery have produced partial success stories, the misdirection of regenerating axons accounts at least partially for relatively poor functional performance results from many therapies. Thus, physical guidance and microenvironment support for regrowing axons are essential for significantly advancing improvement (Gordon et al., 2003; Krick et al.,

2011; Liu et al., 2011). The construction of scaffolds and conduits from synthetic and natural biomaterials to provide axonal guidance support has been a principal approach to improve SCI recovery for decades (Hadlock et al., 2000). These scaffolds/conduits can serve to bridge gap sites in lesioned neural tissue. The importance of this bridging is highlighted by reports such as the presence of axons within trabeculae crossing the lesion, implying that axons, when provided with an appropriate substrate, such as a bridge, will grow into and across an injury site regardless of glial scar presence (Fortun et al., 2009). However, without the perfect parameters to support regenerative guidance, a bridge may not have any effect.

Bridge design parameters include scaffold composition (i.e. mechanical properties), size and shape, biocompatibility, biodegradability, porosity/mesh size, capacity to appropriately house cells or molecules, and capacity to adapt to various needs. Scaffold designs can arguably be divided into two major categories: 1) solid, preformed scaffolds and (2) injectable liquid or gel scaffolds (Bueno et al, 2007; Du et al., 2011; Macaya and Spector, 2012). Approaches that have employed preformed scaffold implantation have utilized materials such as collagen, poly-ε-caprolactone (PCL), polylactic-co-glycolic acid (PLGA), poly-L-lactic acid (PLA), methylcellulose, fibrin, hyaluronic acid (HA), oligo polyethylene glycol fumarate (OPF). Scaffold-fashioning methods have included fiber cross-linking, gelation, and electrospinning (Cholas et al., 2012; Ding et al., 2011; Joo et al., 2012; Liu, et al. 2012; McCreedy & Sakiyama-Elbert, 2012; Saadai et al., 2011; Wei et al., 2010). Compared to solid implantable scaffold materials, injectable materials, such as liquids that become gels or solids, have the advantage of being able to fill physical defects and to form scaffolds with integrative implant-tissue interfaces. Injectable scaffold materials include collagen, agarose, HA, tetronic-oligolactide, chitosan, and poly(N-isoproylacrylamide)-polyethylene glycol. Utilization methods include liquids that

become gels or solids, gels that become solids, liquids that remain as liquids, and gels that remain as gels. Guidance support strategies are frequently used in combination with other strategies, since other facets of SCI lesions are usually disregarded in experiments with only scaffold therapies (Macaya and Spector, 2012).

Cellular Implants

As established, the most successful structural and functional restoration after SCI requires at least neuro-rehabilitation and regeneration. Cellular implants can be used to address both of these restoration requirements. Commonly employed cell types can operably be divided into two major categories: (1) cells that can differentiate into or that already display neural phenotypes typically found in the adult spinal cord and (2) cells that do not differentiate to become or that are not phenotypically imitative of cells typically found in the adult spinal cord (Leung et al., 2012; Novikova et al., 2011; Sandner et al., 2012).

Therapies using cells that can differentiate to or that already display neural phenotypes utilize stem cells (ex. embryonic, fetal, adult mesenchymal, neural, or endothelial) and precursor cells (ex. oligodendrocyte precursor cells), though oligodendrocytes and astrocytes have also been implanted to promote functional recovery (Davies et al., 2011; Erceg et al., 2010). Multi- or pluripotent stem cell strategies are implemented with the hope that the appropriately differentiated neural cells will replace lost cells and will serve to support axonal regrowth and regeneration. Mesenchymal stem cells have been found to enhance remyelination and improve functional recovery of motor skills in rats and dogs (Karaosz et al., 2012; Park et al., 2012; Sandner et al., 2012). Umbilical cord blood stem cells have additionally been shown to upregulate matrix metalloproteinase-2 levels, reducing glial scar formation and further allowing

for axonal regeneration (Veeravalli et al., 2009). Though stem cells have the ability to differentiate into neurons or glial cells and thus exhibit different properties, such as myelination or neurotrophin/neurotropin release, the regulation of stem cell differentiation can be complex and difficult, adding more possible variables to a successful stem cell therapy formula. The use of a mature cell type, that provides myelination and trophic/tropic support to regrowing axons, may have fewer variables, since differentiation would not be a requisite (Karaosz et al., 2012; Sandner et al., 2012).

The other group of cell types commonly used to improve SCI recovery, namely those that are not and cannot differentiate into cells that display adult spinal cord cell phenotypes, includes Schwann cells and olfactory ensheathing cells (Leung et al., 2012; Novikova et al., 2011; Sandner et al., 2012). Both have induced improved functional recovery after SCI in various animal models through either the myelination of unmyelinated axons or the provision of important neurotrophic/neurotropic factors (Deng et al., 2011; Wang et al., 2011; Ziegler et al., 2011).

Other Strategies

Less commonly published strategies include the supplementation of VEGF (Lutton et al., 2012), polyunsaturated fatty acids (Ward et al., 2010), ethyl pyruvate (Yuan et al., 2011), and naturally-occurring anti-inflammatory curcumin (Lin et al., 2011; Ormond et al., 2012). Also, the cellular damage and death induced by oxygen free radicals after SCI has recently been a major target for improving functional recovery after SCI. Antioxidants and free radical scavengers, such as edaravone and resveratrol, have been shown to reduce the effect of free radicals such as nitric oxide, malondialdehyde, superoxide dismutase, and glutathione peroxidase after SCI

(Ozgiray et al., 2012). These and many other approaches, unfortunately, are uni-dimensional in nature, and therefore are suboptimal or require combination. As overviewed, the use of SCs alternatively affords a multi-dimensional approach to SCI recovery, making them strong candidates for inclusion in therapies. Also mentioned earlier, SCs exhibit limited migration and do not provide a way to physically guide regrowing and regenerating axons. Scaffold implantation can supplement this insufficiency while providing a substrate on which to administer cellular or acellular entities, such as SCs.

Chapter 3:

Bioengineering: Electrospinning Scaffolds to Facilitate Axonal Regeneration after SCI

To properly host viable SCs or facilitate any sort of recovery after SCI, scaffolds must meet several requirements. Bioengineering affords the convenience of being able to tailor the scaffold design to the specific demands of the model. Design considerations should first address the ability of a scaffold to independently promote axonal regeneration and functional recovery from SCI, then a scaffold's capability to carry and support therapeutic cells, neurotrophic/neurotropic factors, and other neuroprotective or neuroregenerative compounds, and finally the ability of a combined therapeutic model of scaffold and compound to improve recovery after SCI.

Mimicking the three-dimensional, complex architecture of the nano-, micro-, and macro-environment that constitutes the ECM of the injury site has been a primary goal of recent scaffold fabrication (Gordon et al., 2003; Krick et al., 2011; Liu et al., 2011; Srouji et al., 2008). This pursuit of the ideal scaffold in various SCI models has informed the list of important factors that contribute to scaffold success. These factors include scaffold composition (i.e. material), size and shape, biocompatibility, biodegradability, the capacity to appropriately house exogenous cells or molecules, the capacity to support the survival and directional growth of endogenous neurons and glial cells, and the capacity to adapt to various needs (Bueno et al, 2007; Dewitt et al, 2009; Du et al., 2011; Kim et al., 2007).

Though initially patented in 1934, electrospinning has only recently enjoyed growing popularity. The basic format consists of a blunted needle fitted to a syringe, filled with the dissolved scaffold material, which is mounted onto a machine that controls solution expulsion from the needle. The solution is passed through a graded electrostatic field, generated by a high

voltage (1-50 kV) source, and onto a grounded collector (for fiber deposition). Basic configurable parameters include needle tip-to-target distance, applied voltage, and volume flow rate (of the substance exiting the needle). The grounded collector can either be one solid, uniformly charged metal conductor, in which case the process is referred to as conventional electrospinning, or multiple, equally charged metal conductors separated by air, in which case the process is termed air-gap electrospinning. Both methods have produced scaffolds with neuronal ECM-like properties from a variety of materials (Jha et al., 2011; Srouji et al., 2008).

Several groups have suggested the success of electrospun scaffolds to promoting axonal regeneration and functional recovery after nerve injury. Electrospun PLGA-silk fibroin-collagen scaffolds have been characterized as displaying appropriate hydrophilicity, fiber diameter, and porosity to host therapeutic cells and promote nerve regeneration (Wang et al., 2011). Silk-fibroin electrospun scaffolds have similarly been shown to appropriately host and support cells therapeutic for SCI, such as olfactory ensheathing cells (Shen et al., 2010). Additionally, electrospun resorbable material polydioxanone has been suggested to support neurite outgrowth to different degrees depending on electrospinning-dependent parameters (Chow et al., 2007). Electrospun poly-L-lactic acid fibers have been shown to directionally support axonal regrowth (Schaub & Gilbert, 2011).

Chapter 4:

Schwann Cell Infiltration and Migration into Electrospun Scaffolds

Packed with fiber layers on the micrometer or nanometer scale, electrospun scaffold morphology is highly tunable. Various parameters, such as material, fiber diameter, pore size, and solvent used all affect cellular response to the biomaterial. A major variable is the number of dimensions in which the scaffold is fabricated. Though electrospinning has traditionally produced two-dimensional scaffolds, three dimensions allows for salient, interconnecting pores between nanofibers, thus closely mimicking the native ECM and increasing the likelihood of cell and functional tissue survival (Blakeney et al., 2011).

Cell infiltration and migration into three-dimensional scaffolds have become primary goals for SCI recovery approaches employing seeded or interlaced electrospun scaffolds. An unfortunate, yet characteristic, paradox of the electrospinning process is that it does not afford both optimal cell attachment and cellular infiltration simultaneously, since if porosity is decreased and fiber packing density increased in order to strengthen planar structure and improve cell seeding and attachment, cellular infiltration can be compromised. An easily-altered parameter, scaffold porosity has recently become a popularly researched and published focus. Additionally, its direct effect on cell seeding and infiltration, make it an attractive focus of study (Blakeney et al., 2011; Vaquette, et al., 2011). Recent research on cellular-based combinatorial strategies utilizing electrospun scaffolds to facilitate SCI repair has shown promising advances in the seeding, migration, and infiltration of various cell types, especially SCs (Griffin et al., 2011; Jeffries & Wang, 2012; Wang et al., 2010; Wang et al., 2011).

Current Study

The current study evaluates SC migration into three-dimensional (3D) electrospun scaffolds and hypothesizes that SC migration across two-dimensional (2D) scaffolds, also generated through electrospinning, will be more improved by Matrigel™ than by laminin. We then aim to confirm results from other studies that Matrigel™ and SCs independently improve functional recovery after SCI. Furthermore, we hypothesize that, after a complete transection at the eighth thoracic vertebra (T8) in rats, the combined treatment of Matrigel™, an electrospun guidance and support scaffold, and SCs (seeded and grown on the electrospun scaffold) will more effectively improve recovery, as measured by the restoration of urine volume retained, hindlimb motor control, and body weight, than the independent effect of the electrospun scaffold and the combined effect of Matrigel™ and electrospun scaffold. We hope, through our *in vitro* and *in vivo* studies, to be able to characterize the combination of electrospun polydioxanone, SCs, and Matrigel™ as a strong potential tactic for improving functional recovery after SCI in rats.

METHODS

Schwann Cell Culturing

Primary rat SCs were obtained from Sciencell™ Research Laboratories (Catalog Number (#): R1700). Upon receipt, cells were grown in Schwann cell medium (Sciencell™ Research Laboratories, Catalog #: 1701) to 90% confluency and then passaged up to three times. Cell medium was replaced the day following a passage and every other day afterward until the next passage. Schwann cell purity, as determined by counting immunostained cells, was found to be 95.6% at the first passage, 94.1% at the second passage, and 94.8% at the third passage.

Scaffold Engineering/Construction – Electrospinning

Biomaterial Preparation – Polydioxanone Suture Dissolution

Polydioxanone suture (PDS) (Ethicon™; Catalog Name/Number: PDS* II/Z762D) was cut into three-inch-long pieces and gently shaken and dissolved in 1,1,1,3,3,3-Hexafluoro-2-propanol (HFP) (Oakwood Products, Catalog #: 003409), also referred to as hexafluoroisopropanol (HFIP), at a concentration of 100mg/ml (100mg of PDS in 1mL of HFP) in a 10mL plastic syringe for 20 hours. A blunted-tip, hypodermic needle (18 gauge, 1.5 inches long, Becton Dickinson & Co. PrecisionGlide®) was then fixed to this syringe, which was then fastened into a syringe pump (KD Scientific, Catalog Number: KDS100). The syringe pump flow rate (rate of solution extrusion from needle) for air-gap electrospinning was 9 mL/hour while the flow rate for traditional, or mandrel, electrospinning was 8 mL/hour.

3D Scaffold Material Collection - Air-Gap Electrospinning Setup

The air-gap electrospinning collecting apparatus, onto which charged fibers land after being extruded from the needle, consisted of two separated, identical, static, grounded metal spheres (radius = 1.0 cm) atop plastic poles that raised the stainless steel spheres to the same height as the syringe (for optimized fiber collection). The two spheres were placed 10 cm apart from each other, with two cylindrical rods (length = 2.5 cm, radius = 1.0 mm) as landing targets for the material coming from the needle, extended from each sphere directly towards each other, oriented perpendicular to the orientation of the needle. Thus, a 3.0 cm gap of air for fiber distribution and collection was created between the two rods; it is in this gap that the scaffold was constructed, bridging the ends of the two rods. These rods supported and facilitated the fiber collection and eventual scaffold fabrication. The result was a long, cylindrical, non-woven, fabric-like sheet of polydioxanone fibers of nanometer-scale diameters.

2D Scaffold Material Collection – Conventional (Mandrel) Electrospinning Setup

The collecting apparatus for the traditional electrospinning consisted of one rectangular, grounded spinning (1000 revolutions/min) stainless steel block (80Lx20Wx2H mm) raised to an optimal height to serve as a landing surface for incoming charged fibers and oriented perpendicularly in relation to the syringe and needle. An even, non-woven sheet, resembling fabric, of polydioxanone fiber with nanometer-scale diameters, was dispensed over the block's complete surface.

Scaffold Construction - Electrospinning

For both electrospinning methods, the positive output lead of a high voltage supply (Spellman High Voltage Electronics Corporation; Catalog #: CZE1000R), set to 15 kV for the air-gap method and 20 kV for the conventional (mandrel) method, was attached via alligator clip to the needle on the syringe, while the negative output lead of another high voltage supply, also set to 15 kV, was attached to the collecting apparatus. Spinning duration was 15 minutes, or until the desired radius was achieved, for the air-gap electrospinning method and 45 minutes for the traditional electrospinning method. Two separate, near-identical air-gap electrospun products (3.0 mm long) were fabricated and processed immediately after one another, while only one traditional electrospun product was obtained and processed for experimental use (Figure 1.1).

Air-Gap Electrospun (3D) Scaffold Preparation

Slicing

The 3.0 cm-long cylindrical electrospun polydioxanone product were cut from the 3.0 cm gap between the rods in which the fibers were collected. The scaffold was placed into a clear acrylic David Kopf® Instruments brain blocker (Catalog #: PA001) and 0.75 cm was cut from each end and discarded, since the physical properties of these ends, that were closest to the collecting rods of the air-gap electrospinning apparatus, were markedly different from the center 1.5 cm of the cylindrical scaffold product. This remaining 1.5 cm scaffold centerpiece was carefully, in a steady sawing motion, cut into 1 mm-thick cylindrical pieces that retained the same diameter of the original uncut product. Since two 3.0 cm-long products were fabricated, two 1.5cm centerpieces were obtained. Thus, 30-1 mm-thick scaffolds were sliced, of which 18 were used for *in vivo* rat SCI model experiments, 4 were used for in vitro cell-on-scaffold

characterization experiments, 3 were used for cell migration-through-scaffold experiments, 2 were used for scaffold characterization experiments, and 3 were discarded due to improper slicing or loss of physical integrity during or after slicing. The average diameter ± standard deviation (SD) of the 27 sliced 1mm-thick scaffolds that were experimentally implicated was 3.72 ± 0.07394 mm.

Matrigel™ Coating

All Matrigel™-coating was done in a sterilized cell culture hood (nuAire, Inc.). Room temperature-thawed BD Matrigel™ (BD BioSciences, Catalog #: 356237) was injected into one well of a sterile 96-well plate well (about 75% to the rim). 20 of the 27 total scaffolds were sterilized in a 35mm petri dish 70% EtOH for 30 minutes, allowed to dry, soaked in SC medium for 10 minutes, then dipped in the Matrigel™ -filled well and swirled around by the experimenter via forceps for 30 seconds. After, 20 of the 27 total scaffolds were coated in Matrigel™, scaffolds were then each placed in separate wells of a 96-well plate to await the application of cells or control (cell-free SC medium).

Cell Seeding

All cell seeding was done in a sterilized cell culture hood. Five, of the remaining seven, Matrigel™-free scaffolds were sterilized for 30 minutes in 70% EtOH and then added to separate wells of the same 96-well plate as the aforementioned 20 Matrigel™-coated scaffolds, in a manner that they could be distinguished from the other scaffolds. Cells were prepared for seeding at the first or second passage. SCs were isolated after centrifugation in their first or second passage, resuspended in 100 µL of cell medium, and submitted to a count via

haemocytometer; trypan blue was used to exclude organic debris and dead cells in the count. After a cell density (cells/mL) was obtained, the appropriate amount of cell medium was calculated and then added to the suspension to dilute the solution so that every 6.5 µL of cell-containing medium contained 74,300 cells. This total number of cells to be seeded on each scaffold was determined by calculating how many SCs could spatially fit, without overlapping, on one circular surface of the 1 mm-thick cylindrical scaffold. For this calculation the average area of one scaffold face, from an observed average scaffold diameter of 3.72 mm, was divided by the average area of an SC, which was calculated from an observed average SC diameter of 12 µm. To optimize cell seeding efficiency, or the percent of applied cells (74,300) that were, indeed, seeded onto the scaffold via attachment, it was decided that cells would be seeded onto the scaffolds by pipetting a droplet of cell-containing medium that, when settled around the scaffold, was as small as possible while still fully enveloping the scaffold; this specification was met with a 6.5 µL aliquot. Thus, 6.5 µL of cell-containing medium, at a concentration of 74,300 cells in every 6.5 µL (11,431 cells/µL), was slowly and carefully pipetted onto the top surface of 19 Matrigel™ -coated scaffolds. 6.5 µL of cell-free medium was pipetted onto the surface of 4 Matrigel™-coated and the 2 Matrigel™-free scaffolds, all of which were in separate wells of a 96-well plate which was promptly covered and placed in a sterilized, humidified CO_2 incubator (Sanyo) at 37^{o}C and 5.0% carbon dioxide. After 3 hours (to allow for initial cell attachment), the plate was slowly removed from the incubator, minimizing shaking and liquid movement. Each scaffold was then cautiously picked up via forceps, turned upside-down, and placed back in the same well, so that the side that was previously seeded with cells was facing the bottom of the well, and the un-seeded side was facing upwards. 6.5 µL of cell-containing medium was then applied to upward-facing side of 6 scaffolds that had previously received cells, while the

remaining 19 scaffolds (10 with Matrigel and cells on one side, 4 with only Matrigel™, and 2 with neither Matrigel™ nor cells) received 6.5 µL of cell-free SC medium. Scaffolds were again incubated for 3 hours and then each scaffold-containing well was filled 50% will cell-free SC medium and left to incubate for 5 days. Cell medium was changed daily.

Cryostat Slicing for SC Dispersion Characterization

To profile the extent of migration/infiltration into the 3D scaffolds, three scaffolds were sliced into 25 µm-thick sections, via a cryostat (Thermo Scientific, property of the Microscopy Core Facility, Virginia Commonwealth University). Every other sliced section was discarded so that sections were collected every 50 µm.

Seeding SCs onto Two-Dimensional Traditional Electrospun Scaffolds

Scaffolds were removed from around the rectangular mandrel of the traditional electrospinning apparatus as one sheet and cut, using a single-edge razor blade, into flat, square scaffolds (5 mm x 5 mm). They were sterilized in 70% EtOH for 30 minutes, allowed to dry, soaked in SC medium for 10 minutes, immersed in a 35mm x 10mm petri dish of either 1X tris-buffered saline (TBS) (50mM Tris-Cl + 150mM NaCl), as the control, laminin, or Matrigel™, and left in a sterile environment overnight (16 hours). Scaffolds were placed into separate wells (of a 48-well culture plate well). SCs were isolated after centrifugation in their third passage, resuspended in 50 µL of cell medium, and submitted to a count via haemocytometer; trypan blue was used to exclude organic debris and dead cells in the count. After a cell density (cells/mL) was obtained, the appropriate amount of cell medium was calculated and then added to the suspension to dilute the solution so that every 1.0 µL of cell-containing medium contained

20,000 cells. 20,000 cells were pipetted onto the visually-determined center of each 5 x 5 mm square, each in their own well. 100 µL of cell-free cell medium was pipetted around the base of each scaffold-containing well to keep scaffolds hydrated, after which the whole 48-well plate was incubated at 37^{o}C and 5.0% carbon dioxide.

The Surgical Implantation of Scaffolds into Animals

Scaffold Preparation

Prepared scaffolds were removed from incubation after 5 days and split into seven experimental groups, including 5 groups implicated in *in vivo* experiments via surgical implantation (N=4 for all 5 groups, unless otherwise noted):

(1) scaffold + Matrigel^{TM} + SCs on both sides;

(2) scaffold + Matrigel^{TM} + SCs on one side (implanted with cellularized side facing rostrally);

(3) scaffold + Matrigel^{TM} + SCs on one side (implanted with cellularized side facing caudally);

(4) scaffold + Matrigel^{TM} + control treatment (SC medium);

(5) scaffold + control treatment (SC medium) (N=2);

For simplification, for the remainder of the paper, all 3D scaffolds that were implanted into animals (*in vivo*) will be referred to as "bridges". The above groups will thus forth be referred to as the following:

(1) SC bridges (both sides);

(2) rostrally-facing SC bridges;

(3) caudally-facing SC bridges;

(4) Matrigel^{TM}-only bridges;

(5) control bridges;

All bridges were washed 3 times for 3 minutes each in Hank's Balanced Salt Solution (HBSS) prior to implantation. Accordingly, 18 rats were split into 5 groups: 4 groups (N=4) + 1 group (N=2).

Surgical Procedure - Complete Spinal Cord Transection

Adult female, Long Evans Hooded rats, of mean (SD) weight = 308.4 (16.5)g, acquired from Harlan Inc, were used partially because of the reported decreased incidence of urinary tract infections in female, compared to male, rats after SCI, and because of the easily manageable behavioral traits of Long Evans Hooded rats, compared to other common experimental strains, to allow for easy daily bladder expression and handling. Bladder expression was necessary because of abnormally high urine retention and lack of auto-expression post-SCI. All surgical procedures were performed in accordance with the guidelines set forth by the Institutional Animal Care and Use Committee. Animals were anesthetized in a clear, sealed container with 5% isoflurane, shaved (from lower-back to shoulders), and fitted into a stereotaxic surgical apparatus (Stoelting) without the manipulator arms. After 2-3 minutes of stable isoflurane administration and testing for complete anesthesia via toe and tail pinches, isoflurane dosage was reduced to 2-3%, betadyne was applied to the shaved skin area, and a percutaneous dorsal, midline incision of about 4 cm was made above the mid-thoracic spine with a scalpel (No. 10 blade), exposing a thick layer of fat which was partially removed to expose the layer of muscle covering the spine. Incisions were made bilaterally of the spinal column and the protective muscle was forced aside and further separated by stainless steel tissue spreaders (Codman) to further isolate the spinal

column and increase the working area. Stainless steel tissue forceps (Codman) were used to clear inter-process tissue and lempert bone rongeurs were used to perform a conventional laminectomy, in which the lamina, along with the rest of the spinal column's posterior backbone, was removed at the eighth thoracic vertebra (T8), fully exposing the dura mater (dura)-encased spinal cord (Figure 1.2a). A complete spinal cord transection was performed using micro-scissors, resulting in two nerve stumps (one rostral and one caudal to the transection site) separated by a less than 1mm gap. An HBSS-washed 1 mm-thick cylindrical scaffold, from one of the five groups identified in "Scaffold Preparation" above, was implanted between the two stumps, serving as a bridge (Figure 1.2b). Following implantation, separated muscle layers were pulled back and sewn together using silk suture (Ethicon Perma-Hand Silk, Catalog #: 682G). Surgical staples were used to close the skin incision. After removal from the surgical apparatus, the animals were placed on an electrical heating pad to counteract any body temperature drops and visually monitored until consciousness was regained. Rats were administered 2 mL of gentamicin sulfate (GentaFuse [Butler], diluted to 1 mg/mL in 9g/L (normal) saline) and 0.25 mL of buprenorphine (0.5 mg/kg); 5 mLs of liquid acetaminophen (150 mg/kg) was diluted into the each animal's drinking water container. Rats were visually monitored for consciousness and forelimb activity every 10 minutes for up to one hour, or until stable.

Post-Operative Animal Care

Rats were housed in separate cages and administered 2 mL of gentamicin sulfate (1 mg/mL) every 12 hours for 7 days and 0.25 mL of buprenorphine (0.5 mg/kg) every 12 hours for 48 hours; liquid acetaminophen remained diluted in rats' drinking water containers for 3 days, and then replaced with plain tap water. Rats were individually monitored (for general

appearance/health and urine color) and their bladders depressed by experimenter hand every 12 hours, while body weight and results from a four sub-scale score of moribundity were taken every 24 hours (moribundity was measured using a 3-point scale, from 0 (normal) to 2 (severe), of appearance, weight, eyes, and activity . Expressed urine volume and pH was measured every 48 hours. pH measurements were stopped after 8 days of a consistent pH measurement of 7, though all other measures were taken for the duration of the animal's life. Drop-wise clindamycin (25 mg/ml) was administered to effectively halt self-mutilation behavior.

Locomotor Activity Testing

Hindlimb locomotor activity and motor control was assessed via a double-blind employment of the 22-point Basso-Beattie-Bresnahan (BBB) Locomotor Rating Scale (Figure 1.3), with 21 constituting complete mobility and 0 constituting complete hindlimb paralysis. The BBB scale considers parameters such as joint mobility, weight support, limb coordination, and gait stability. Rats were placed in a circular open field (radius ~ 38 cm; plastic, light-brown tabletop with a bounded perimeter) and allowed to freely perambulate the tabletop surface for a three-minute time period (Figure 1.4). Animals were scored pre-surgery and immediately post-surgery to establish baseline scores. Then, animals were scored every 4 days. Raw BBB scores represent an average of two independent scorers (the averaged score range never surpassed ±1 from this raw score; ex. a raw score of 8 might have been averaged from independent observer scores of 7 and 9, but not 6 and 10).

Immunostaining, Imaging, and Slicing – In Vitro Analysis

To quantify cell-seeding efficiency, all non-implanted scaffolds with SCs were fixed in 4% paraformaldehyde at the appropriate time points (5 days after seeding for 3D air-gap electrospun scaffolds; 0, 3, 5, and 7 days after seeding for 2D traditionally electrospun scaffolds). Cells were then co-stained for cell nuclei and the intracellular (IC) protein families S100A and S100B, which were used to identify SCs (Mata, Alessi, and Fink, 1990). For SC identification via the S100 protein, cells were permeabilized using 0.25% Triton X-100 and 1% bovine serum albumin (BSA) was used as a blocking agent. The whole cell-seeded scaffold was incubated, overnight at 4^{o}C, in diluted primary antibody S100 (polyclonal anti-rabbit) (Dako, Catalog #: Z0311) at a dilution factor of 1:800 (in phosphate-buffered saline (PBS)-diluted permeabilizing and blocking agents). The scaffold was then incubated, for 1 hour in the dark at room temperature, in diluted secondary antibody AlexaFluor 568 (goat, anti-rabbit IgG) (Invitrogen, Catalog #: A-11036) at a dilution factor of 1:200 (in PBS-diluted permeabilizing and blocking agents). Scaffolds were then stained for nuclei using a 1:1000 dilution factor of bisbenzimide for 2 minutes (courtesy of Dr. Jeff L. Dupree, Ph.D., Virginia Commonwealth University). Samples were then imaged using either a laser scanning confocal microscope (Leica TCS-SP2 AOBS CLSM, property of the Microscopy Core Facility, Virginia Commonwealth University) or a scanning electron microscope (Zeiss EVO 50 XVP SEM, property of the Microscopy Core Facility, Virginia Commonwealth University). For 3D cell migration studies, scaffolds were immunostained, sliced, and then imaged using laser scanning confocal microscopy.

Data Analysis

Cell Quantification

The quantification of cells was done by manually counting SCs (identified by co-localized nuclei and S100 protein family fluorescence after immunostaining and imaging) in a given area and then extrapolating that cell number per unit area to the area of the scaffold surface. This was done at four identical locations on all scaffolds and total cell numbers were calculated as averages of the four sample counts to control for experimenter bias.

Statistical Analyses

One-way analyses of variance tests, along with Tukey's Multiple Comparisons post-hoc tests, were used to analyze mean differences across all groups and the compare each separate group to each other separate group in *in vitro* cell migration and *in vivo* SCI model experiments. Two-way repeated measures analyses of variance tests, along with pairwise Holm-Sidak Multiple Comparison post-hoc tests, were used to determine the effect of different treatments at different time-points. Means were expressed alongside standard deviations or standard errors of mean, as specified in each instance. Also, Spearman correlational analyses were performed to identify the relationship between two functional measures across all treatment groups.

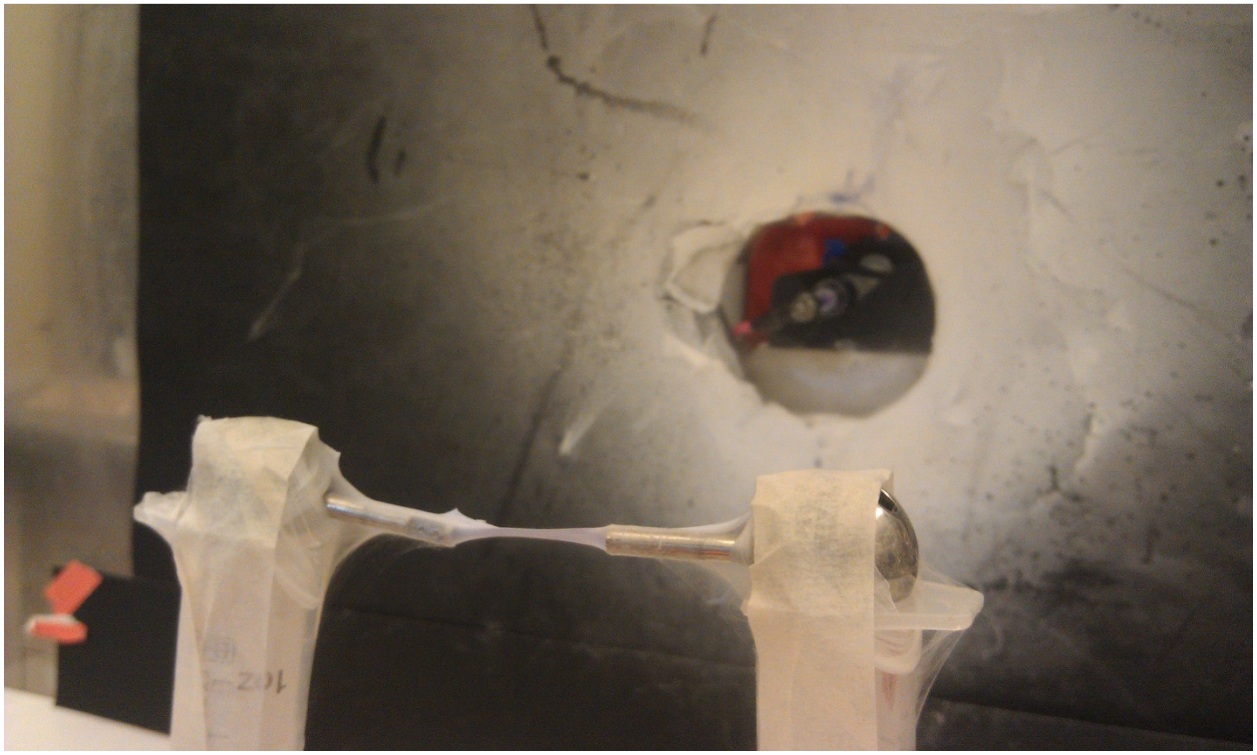

Figure 1.1 Air-gap electrospun product. View of the electrospinning polydioxanone cylindrical product (~3.0mm long) on the collecting apparatus. This represents a point about halfway through the construction process. In the back of the photo is the needle from which the material is being extruded.

(a)

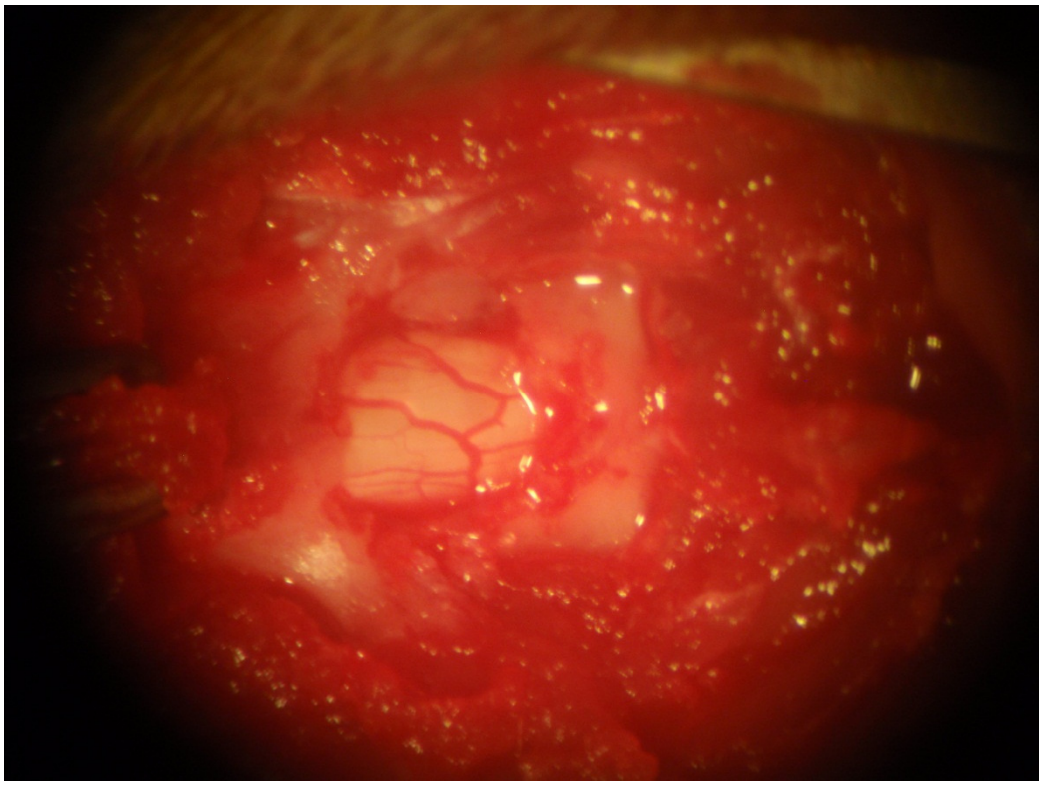

(b)

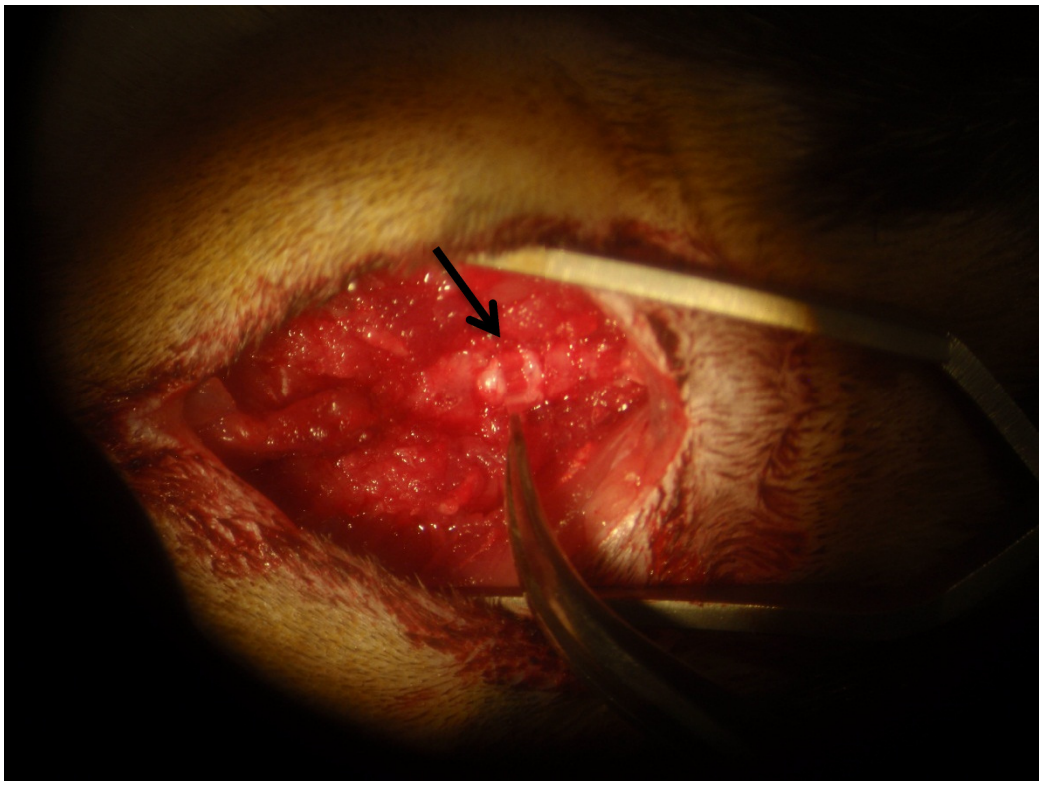

Figure 1.2 The exposed rat spinal cord before transection and after implantation. (a) View of the dura-encased, exposed rat spinal cord before a complete transection. (b) View of the implanted 1mm-thick cylindrical scaffold held in place the pressure of the two stumps rostral and caudal to the transection site. The black arrow indicates this implanted scaffold (between the two white cord stumps).

Rating	Description of Locomotion
0	No observable hindlimb (HL) movement
1	Slight movement of one or two joints (usually hip &/or knee).
2	Extensive movement of one joint or Extensive movement of one joint **and** slight movement of one other joint.
3	Extensive movement of two joints.
4	Slight movement of all three joints of the HL.
5	Slight movement of two joints **and** extensive movement of the third.
6	Extensive movement of two joints **and** slight movement of the third.
7	Extensive movement of all three joints of the HL.
8	Sweeping with no weight support or Plantar placement of the paw with no weight support.
9	Plantar placement of the paw with weight support in stance only (i.e. when stationary) or Occasional, Frequent or Consistent weight supported dorsal stepping and no plantar stepping.
10	Occasional weight supported plantar steps, no FL-HL coordination.
11	Frequent to consistent weight supported plantar steps **and** no FL-HL coordination.
12	Frequent to consistent weight supported plantar steps **and** occasional FL-HL coordination.
13	Frequent to consistent weight supported plantar steps **and** frequent FL-HL coordination.
14	Consistent weight supported plantar steps, consistent FL-HL coordination; **and** Predominant paw position during locomotion is rotated (internally or externally) when it makes **initial contact** with the surface as well as just before it is **lifted off** at the end of stance or Frequent plantar stepping, consistent FL-HL coordination and occasional dorsal stepping.
15	Consistent plantar stepping and Consistent FL-HL coordination; **and** No toe clearance or occasional toe clearance during forward limb advancement, Predominant paw position is parallel to the body at initial contact.
16	Consistent plantar stepping and Consistent FL-HL coordination during gait; **and** Toe clearance occurs frequently during forward limb advancement Predominant paw position is parallel at initial contact and rotated at lift off
17	Consistent plantar stepping and Consistent FL-HL coordination during gait; **and** Toe clearance occurs frequently during forward limb advancement, Predominant paw position is parallel at initial contact **and** lift off.
18	Consistent plantar stepping and Consistent FL-HL coordination during gait; **and** Toe clearance occurs consistently during forward limb advancement, Predominant paw position is parallel at initial contact and rotated at lift off
19	Consistent plantar stepping and Consistent FL-HL coordination during gait; **and** Toe clearance occurs frequently during forward limb advancement. Predominant paw position is parallel at initial contact and lift off and Tail is down part or all of the time.
20	Consistent plantar stepping and Consistent coordinated gait; Consistent toe clearance Predominant paw position is parallel at initial contact and lift off; **and** Trunk instability, tail consistently up.
21	Consistent plantar stepping and Coordinated gait, consistent toe clearance, Predominant paw position is parallel throughout stance, consistent trunk stability **and** Tail consistently up.

Figure 1.3 The Basso, Beattie, Bresnahan (BBB) locomotor rating scale. The 22-point scale used to score locomotor function in an open-field (Basso, Beattie, and Bresnahan, 1995).


HIGH FIVE
Kimwipes

Figure 1.4 The open-field to obtain locomotor scale scores. The radius of the circular open-field used to test locomotor activity was about 38 cm. Rats were allowed to freely roam this space for 3 minutes while two observers watched for parameters defined by the BBB Locomotor Scale.

RESULTS

SC Surface-Attachment onto 3D Scaffolds was Substantial, However SC Dispersion Was Limited

Air-gap electrospun, 1 mm-thick scaffolds, that underwent an identical seeding procedure to those that were implanted into animals, were evaluated for their ability to house cells on their surface in terms of the percent of cells that were initially seeded onto the surface. Of the number of cells that were initially seeded, 63.036% were present after a 5-day CO_2 incubation (mean (SD) = 46,836 (3,983), N = 2) (Figure 2.1a-b; Figure 2.2a-d).

In characterizing dispersion through air-gap electrospun PDS scaffolds, we found an average of 75.128% (mean (SD) = 131,474 (30,044), N=3) of initially seeded cells to be present on the scaffold surface, 37.461% (mean (SD) = 65,556 (16,908), N=3) of seeded cells to be present at a 250 µm depth into the scaffold, and 3.902% (mean (SD) = 6,828 (6,002), N=3) to be present at a depth of 500 µm into the scaffold. All cell counts were obtained from cell-seeded scaffolds that had been fixed 5 days post-seeding in 4% paraformaldehyde (Figure 2.3; Figure 2.4a-b). A comparison of the difference in cell numbers at the surface, 250 µm into the scaffold, and 500 µm into the scaffold revealed ample mean differences ($p<0.001$ [$p=0.0009$], $df = 2$, $r^2 = 0.9050$). Post-hoc analyses show that these large differences were evident not only across all groups, but between each pair of groups as well (Surface vs. 250 µm ($p<0.05$), Surface vs. 500 µm ($p<0.001$), and 500 µm vs. 250 µm ($p<0.05$)).

Matrigel™, Slightly More Than Laminin, Facilitated 2D Cell Dispersion

Matrigel™-, laminin-, and TBS (control)-coated 5 mm x 5 mm traditionally electrospun scaffolds were assessed for their ability to facilitate two-dimensional SC dispersion. Cells on

Matrigel™-coated scaffolds migrated over mean areas (SEMs) 2.341 (0.09185) times, 3.154 (0.1018) times, and 4.050 (0.1689) times as expansive as the area covered by initially seeded cells (at Time (T) = 0 days) at 3, 5, and 7 days post-seeding, respectively. Likewise, cells on laminin-coated scaffolds migrated over areas 1.656 (.07490) times, 2.188 (0.04527) times, and 2.867 (0.01789) times that of initially seeded cells, at 3, 5, and 7 days, respectively. These were compared to each other and to a control (a TBS-coated scaffold), which yielded cell dispersion 1.284 (0.04440)x, 1.787 (0.1733)x, and 2.420 (0.1517)x, that of the T = 0 cell area at 3, 5, and 7 days post-seeding, respectively. Though there was no difference ($p = 0.3440$, $df = 2$, $r^2 = 0.2111$) between means of cell-covered areas of Matrigel™-coated, laminin-coated, and TBS-coated scaffolds (Figure 2.5a-f). There was, however, a clear trend of cells covering increasingly greater areas on Matrigel™-coated than on laminin-coated scaffolds and on laminin-coated than on TBS-coated scaffolds.

Animals

Animal responses to the complete transection surgery were consistent in the following general features. All rats lost 10-30% of their pre-surgery body weight within 7 days of the surgical procedure. Also, all rats became bloated within 10 hours of the surgery, due to distending, unrelieved bladders due to the loss of micturition control. As expected, all rats also lost all sensory perception and motor control caudal of the transection site. There were also several variable factors among the rats. About one-third of the rats performed some degree of self-mutilation at the level of the skin (i.e. attempting to chew through its own dermal layers) in the area of the peritoneum. Others developed short-term urinary tract infections, identified by putrid-smelling, brown-colored urine. Throughout the course of the study, two rats were euthanized due to extensive self-mutilation, while one died of an unknown cause.

SC-Seeded Electrospun PDS Bridges Affect Animal Body Weight Restoration after SCI

All experimental *in-vivo* groups were evaluated for their differences in ability to restore lost animal body weight after a complete spinal cord transection (the control bridge group was excluded due to low sample size and evidence for surgical error). When compared to every other group, animals that received implants of SC bridges (both sides) regained a higher percentage of their pre-surgery body weight ($p<0.0001$, $df = 4$, $r^2 = 0.1742$). Interestingly, post-hoc analyses showed that this group showed larger mean differences when compared to animals with caudally-facing bridges ($p<0.0001$) and Matrigel^{TM}-only bridges ($p<0.0001$) than when compared to animals with rostrally-facing bridges ($p<0.001$) (Figure 2.7). As confirmed by the figure, no other groups differed from each other.

SC-Seeded Electrospun PDS Bridges Do Not Affect Retained Urine Volumes after SCI

Experimental *in-vivo* groups were assessed for differences in overall bladder function restoration as well as time taken to achieve this restoration (the control bridge group was excluded due to low sample size and evidence for surgical error). Means of retained urine volumes between groups were not found to be different ($p<0.4525$, $df = 4$, $r^2 = 0.06133$) (Figure 2.8). Analyses of the number of days until active micturition or until achieving a retained urine volume of zero also yielded no differences between groups ($p<0.2149$, $df = 4$, $r^2 = 0.3614$) (Figure 2.9). However, results yield a trend for animals with SC bridges (both sides) to have regained micturition control over a shorter time period than scaffolds with rostrally- and caudally-facing SC bridges. Additionally, animal groups with both rostrally- and caudally-facing

SC bridges regained this control over a shorter time period than did animals with Matrigel™-only bridges (Figure 2.9).

SC-Seeded Electrospun PDS Scaffolds and Matrigel™-Coated Scaffolds Effect the Gain of Locomotor Function after SCI

Groups were then compared to evaluate differences in the regain of locomotor function, as measured by the BBB scale. In comparing treatment groups, between-group mean differences were revealed ($p<0.0001$, $df = 4$, $r^2 = 0.3390$). Specifically, differences were found between animals with SC bridges (both sides) and with control bridges ($p<0.0001$), between animals with SC bridges (both sides) and with rostrally-facing SC bridges ($p<0.01$), and between animals with Matrigel™-only bridges and with control bridges ($p<0.01$) (Figure 2.10). Analyzing the effect of treatment groups across time, we found no difference until post-surgical day 28, at which point differences were first seen between the SC bridge (both sides) and the control bridge groups ($p<0.01$) and continued in these groups until the final time-point of 44 days ($p<0.001$ at 32 days onwards). At 32 days, differences were also seen between SC bridge (both sides) and rostrally-facing SC bridge animals ($p<0.05$) as well as SC bridge (both sides) and Matrigel™-only bridge animals ($p<0.05$). These differences increased from 36 to 44 days ($p<0.001$). At day 36, differences were also seen between SC bridge (both sides) and caudally-facing SC bridge animals ($p<0.001$). Differences appeared between control bridge and rostrally-facing SC bridge groups ($p<0.05$), rostrally-facing and caudally-facing SC bridge groups ($p<0.05$), and Matrigel™-only and caudally-facing SC bridge groups ($p<0.05$) at 40 days and became more pronounced ($p<0.01$, $p<0.001$, $p<0.01$, respectively) at 44 days. At 44 days, differences between control bridge and Matrigel™-only groups appeared ($p<0.05$).

Body Weight Restoration is Related to Functional Locomotor Activity Restoration

Since only the rats with SC bridges (both sides) displayed differences in more than one assessment (body weight restoration and locomotor function recovery), this group was used to determine the degree of co-variation between locomotor (BBB) scale scores and percent of initial body weight lost over time. We found that the percent of initial body weight lost was, indeed, negatively-correlated with BBB scores (Pearson $r = -0.6496$, $p = 0.0222$ [$p<0.05$], $r^2 = 0.4220$) (Figure 2.11).

(a)

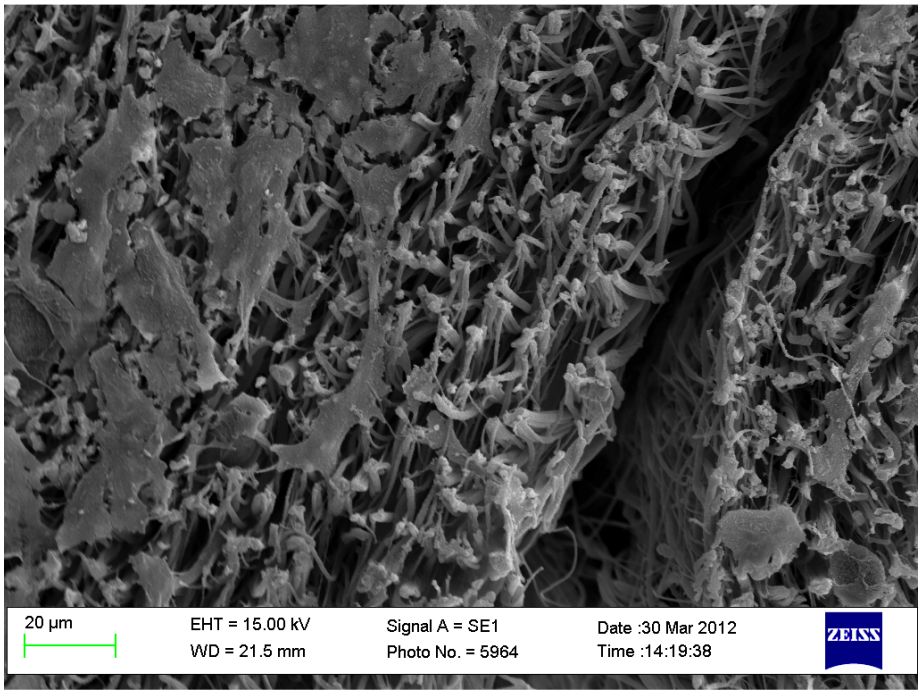
20 µm
EHT = 15.00 kV
WD = 21.5 mm
Signal A = SE1
Photo No. = 5964
Date :30 Mar 2012
Time :14:19:38
ZEISS

(b)

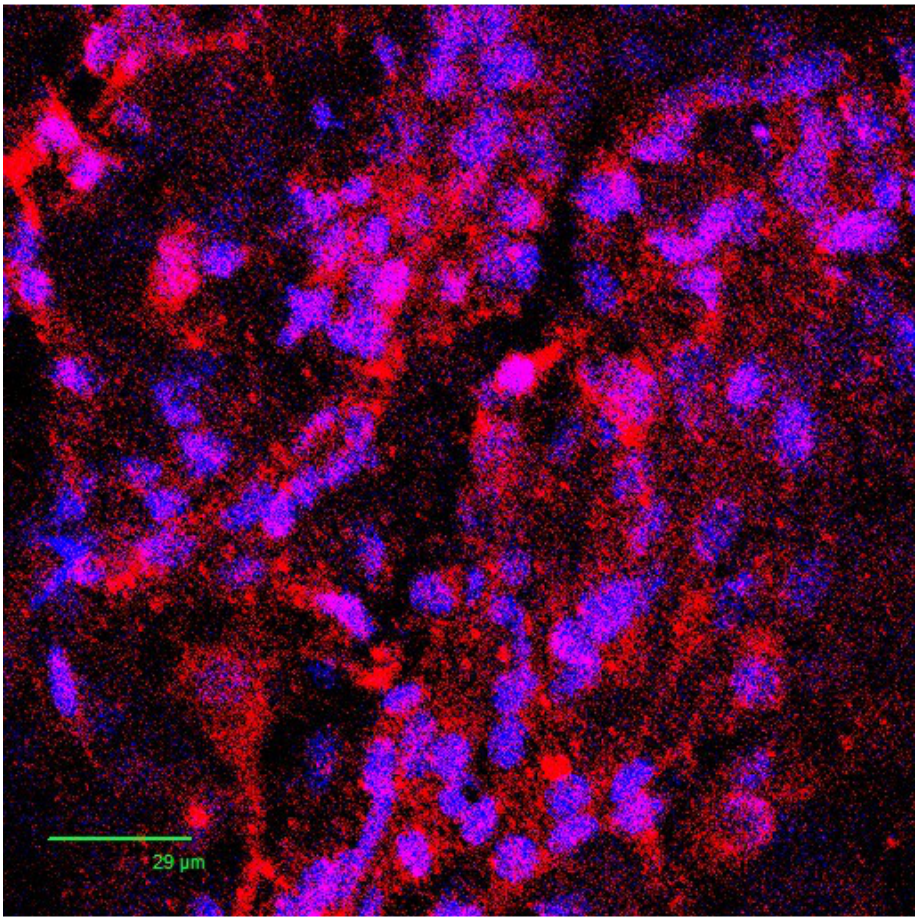
29 µm

Figure 2.1 Images of SCs attached to the surface of the 1mm-thick cylindrical electrospun polydioxanone scaffold. (a) Scanning electron microscopy was used to image the exterior of cells atop electrospun scaffolds after five days of incubation post-cell-seeding. Scaffold and cells were fixed in 4% paraformaldehyde, dried, gold-sputtered, and then imaged. (b) Confocal laser scanning microscopy was used to image fluorescently stained protein S100 (for SCs) (red) and nuclei (blue). The overlapping of the co-stain thus results in a purple- or pink-like color. Cells are atop electrospun scaffolds on which they incubated for five days post-cell-seeding before being fixed in 4% paraformaldehyde and then stored in 1X PBS until imaged.

(a)

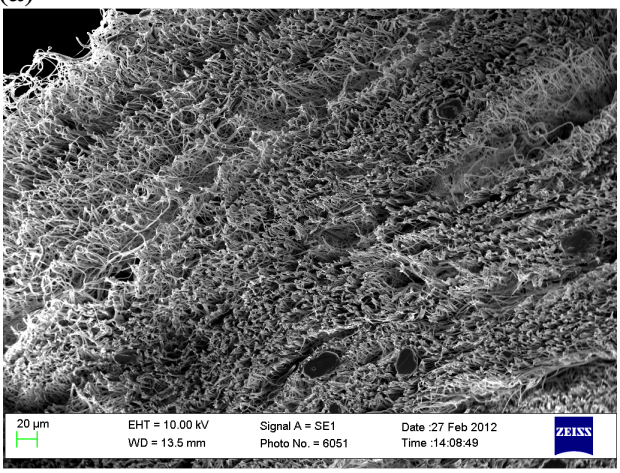
20 µm
EHT = 10.00 kV
WD = 13.5 mm
Signal A = SE1
Photo No. = 6051
Date :27 Feb 2012
Time :14:08:49
ZEISS

(b)

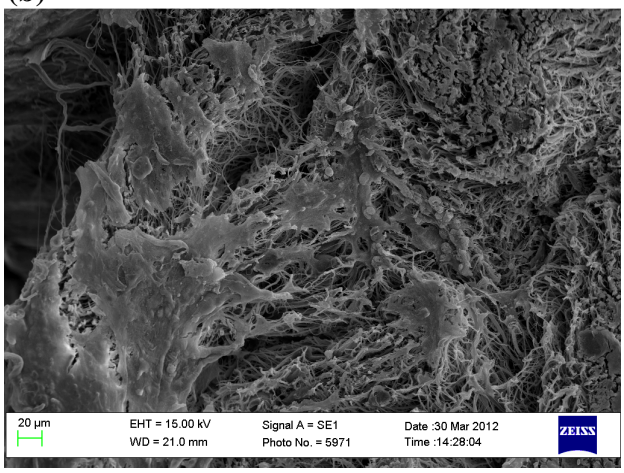
20 µm
EHT = 15.00 kV
WD = 21.0 mm
Signal A = SE1
Photo No. = 5971
Date :30 Mar 2012
Time :14:28:04
ZEISS

(c)

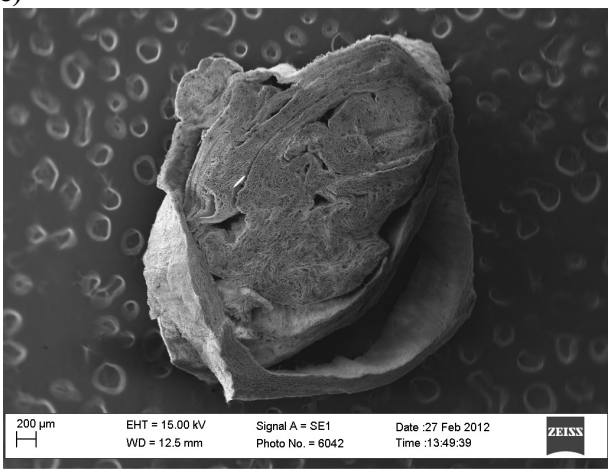
200 µm
EHT = 15.00 kV
WD = 12.5 mm
Signal A = SE1
Photo No. = 6042
Date :27 Feb 2012
Time :13:49:39
ZEISS

(d)

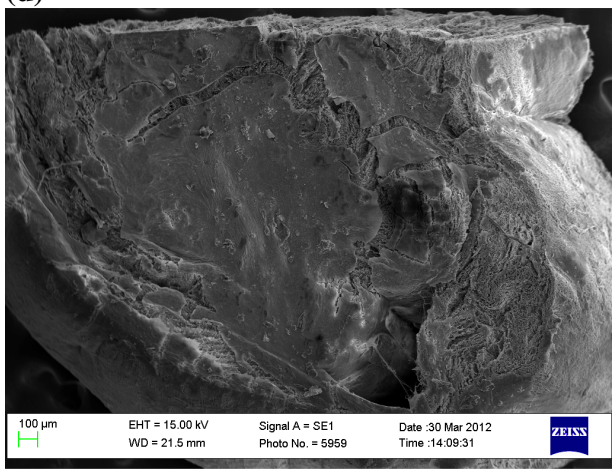
100 µm
EHT = 15.00 kV
WD = 21.5 mm
Signal A = SE1
Photo No. = 5959
Date :30 Mar 2012
Time :14:09:31
ZEISS

Figure 2.2 Scanning electron microscopy photographs of electrospun scaffold surfaces with and without attached SCs. (a) Air-gap electrospun scaffold sliced into a 1 mm-thick cylindrical piece. Fibers can be seen pointing straight up at the observer, and are arguably partially aligned (b) As in panel (a), an air-gap electrospun scaffold sliced into a 1 mm-thick cylindrical piece is seen, however much of the shown surface is covered in a thick cell layer, formed after five days of incubation post-seeding. Cell can be seen growing out from the cell layer. (c) A characterization of a whole scaffold, which an outer layer pulled away from the core scaffold piece to show its layer-like construct. As can be seen, the scaffold is diversely constructed in different areas. (d) As in panel (b), a thick cell layer, or a culmination of many cell layers, can be seen covering a large percentage of the scaffold surface.

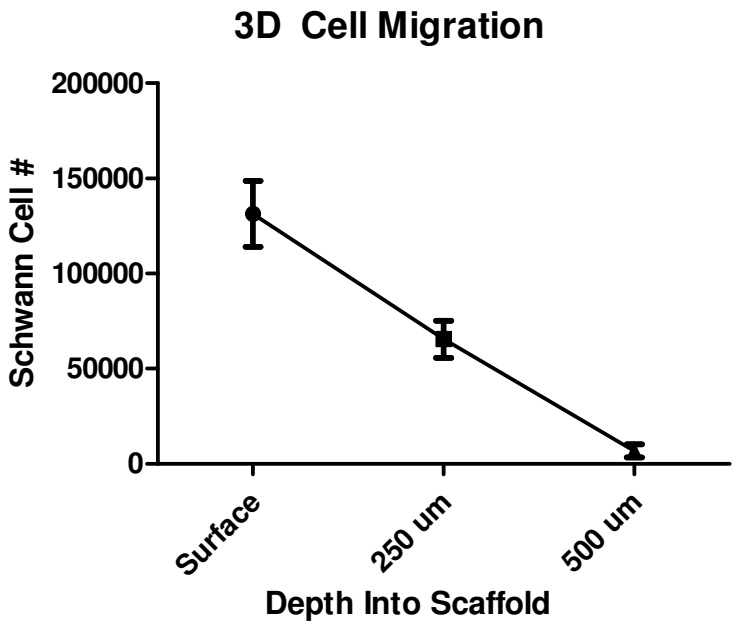
3D Cell Migration
200000
150000
100000
50000
0
Schwann Cell #
Surface
250 um
500 um
Depth Into Scaffold

Figure 2.3 The migration/infiltration of cells into a 3D scaffold. Scaffold were immunostained, sliced, via cryostat, and imaged, via confocal laser scanning microscopy, at the surface, at a depth of 250 µm into the scaffold, and at a depth of 500 µm into the scaffold. These are the extrapolated cell counts calculated from fluorescent images of smaller areas on the scaffolds (N=3)

(a)

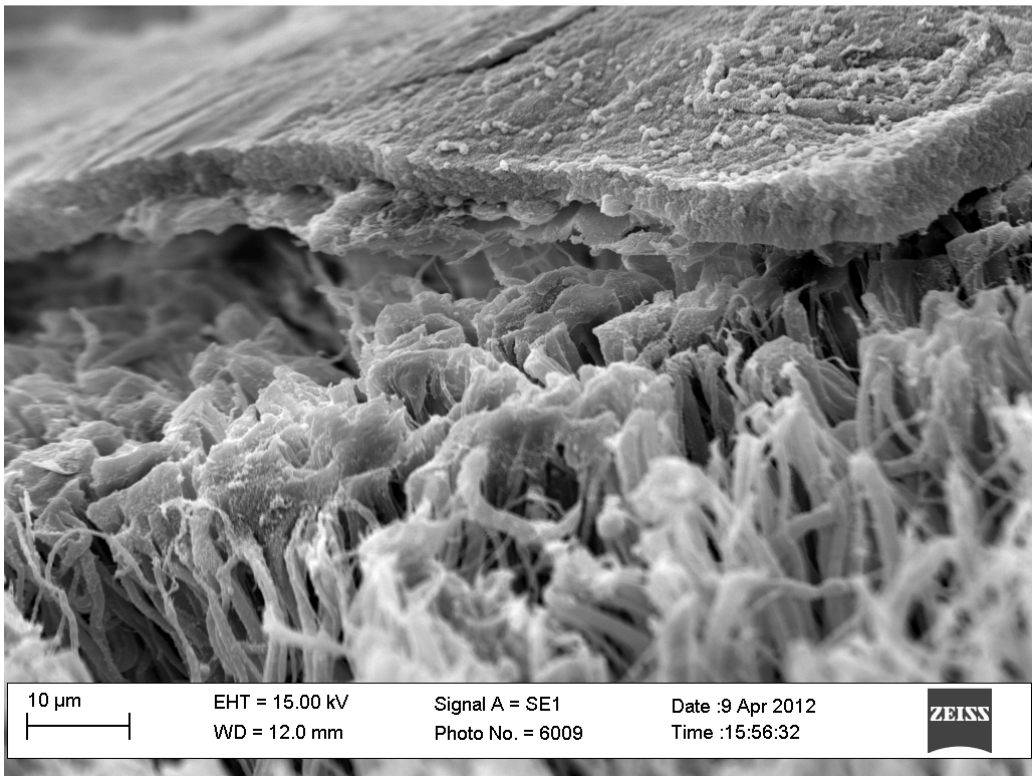
10 µm
EHT = 15.00 kV
WD = 12.0 mm
Signal A = SE1
Photo No. = 6009
Date :9 Apr 2012
Time :15:56:32
ZEISS

(b)

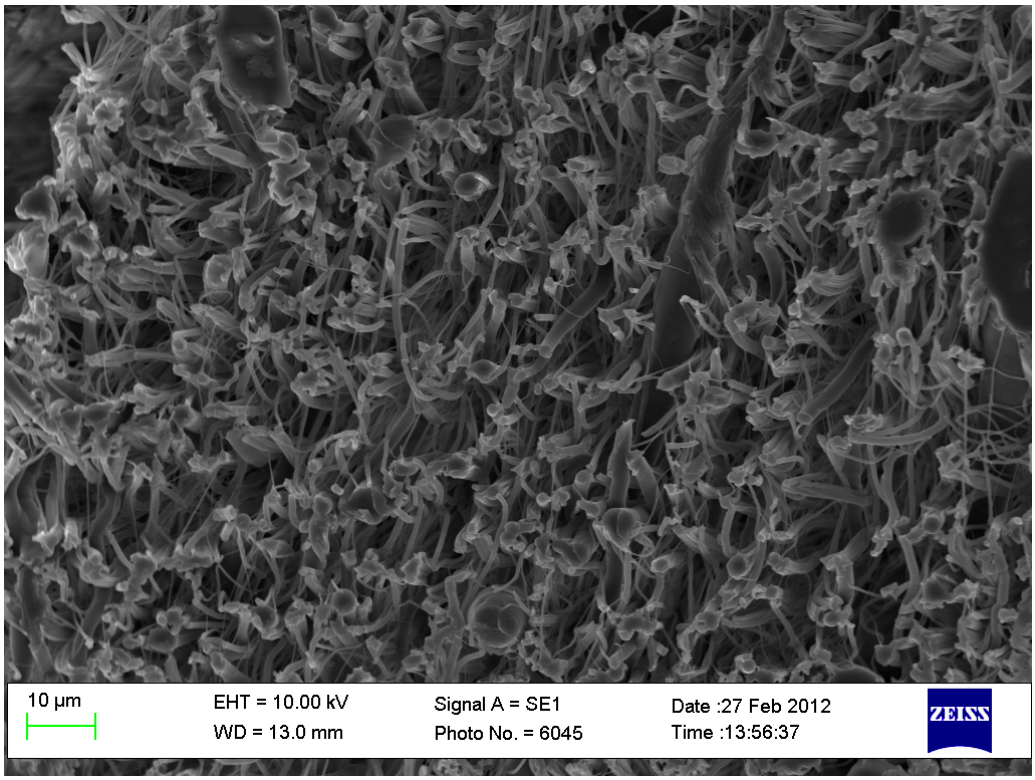
10 µm
EHT = 10.00 kV
WD = 13.0 mm
Signal A = SE1
Photo No. = 6045
Date :27 Feb 2012
Time :13:56:37
ZEISS

Figure 2.4 Scanning electron microscopy photographs of electrospun scaffolds with and without cells. (a) Cells have formed a thick layer atop of the scaffold, signifying robust growth at the surface. Cells seem to be beginning to infiltrate the scaffold, but mainly remaining on the surface. (b) A similar view of a scaffold without cells is displayed to compare with the cell-seeded scaffold to positively and reliably distinguish scaffold material from cells.

Control (TBS)	(+) Laminin	(+) Matrigel
(a)	(e)	(i)
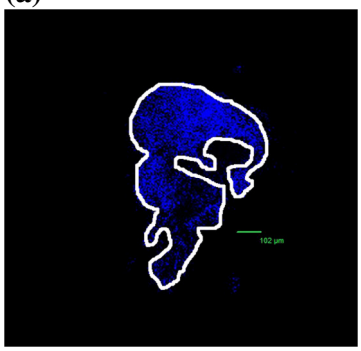	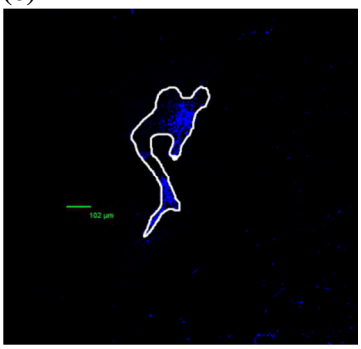	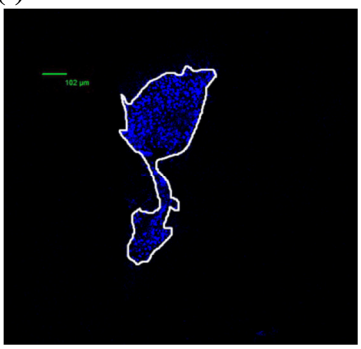
T= 0 days	0 days	0 days
(b)	(f)	(j)
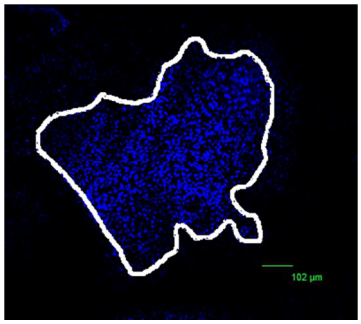	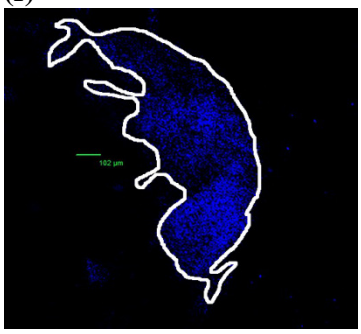	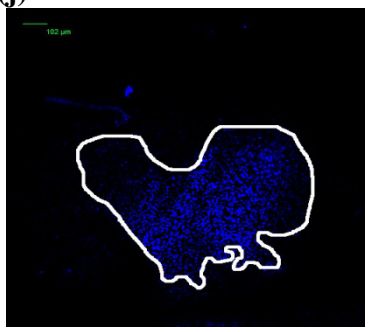
T= 3 days	3 days	3 days
(c)	(g)	(k)
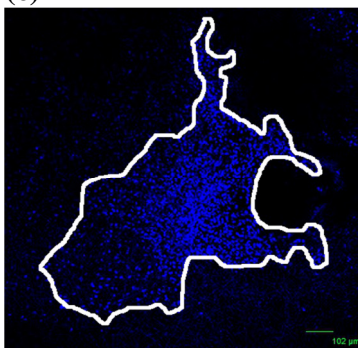	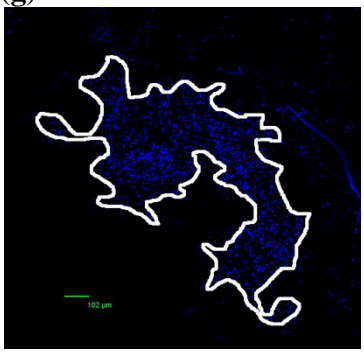	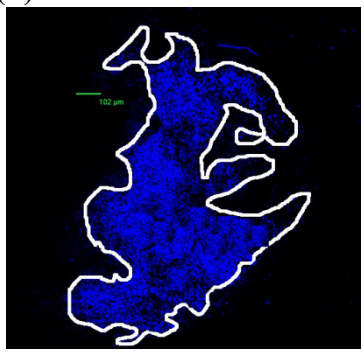
T= 5 days	5 days	5 days
(d)	(h)	(l)
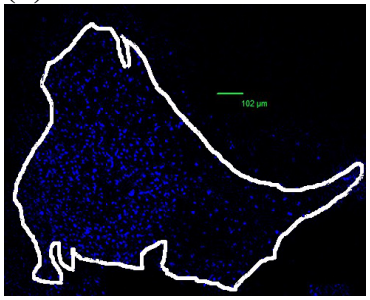	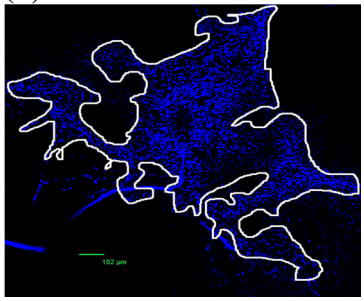	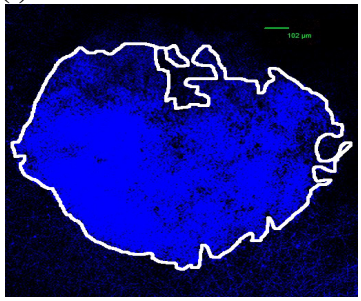
T= 7 days	7 days	7 days

Figure 2.5 Fluorescent images of SC cell nuclei for cells progressively migrating in two dimensions over time and on different substrates. Cell-containing areas are outlined in white. SC dispersion on a TBS (control)-coated scaffold at (a) 3 hours post-seeding (T=0), (b) 3 days post-seeding, (c) 5 days post-seeding, and (d) 7 days post-seeding. SC dispersion on a laminin-coated scaffold at T= (e) 0 days, (f) 3 days, (g) 5 days, and (h) 7 days. SC dispersion on a Matrigel-coated scaffold at T= (i) 0 days, (j) 3 days, (k) 5 days, and (l) 7 days.

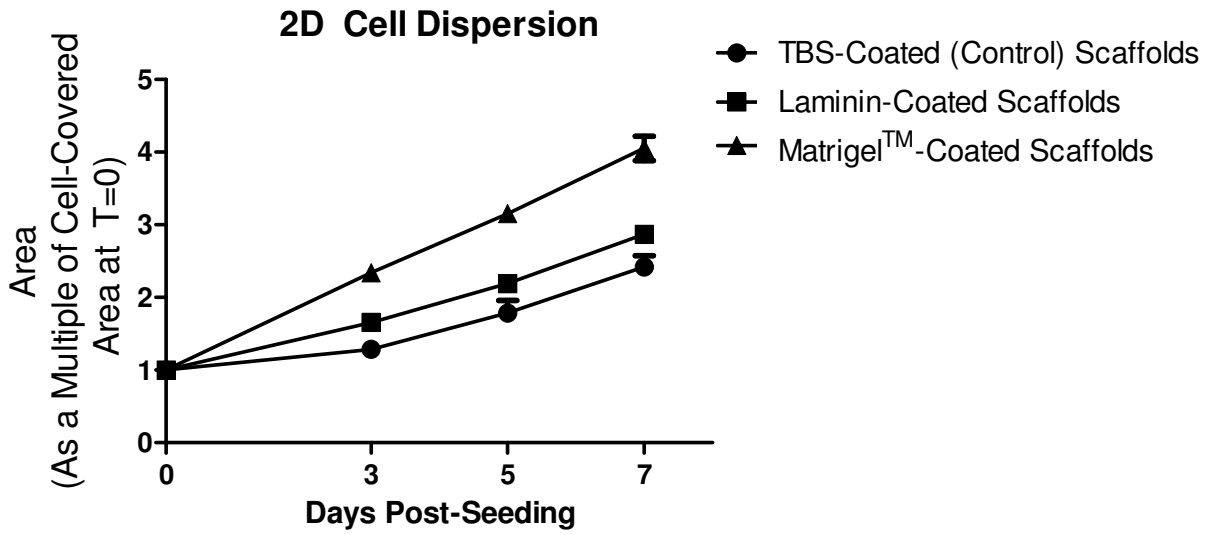
2D Cell Dispersion
Area
(As a Multiple of Cell-Covered Area at T=0)
0
1
2
3
4
5
0
3
5
7
Days Post-Seeding
TBS-Coated (Control) Scaffolds
Laminin-Coated Scaffolds
Matrigel™-Coated Scaffolds

Figure 2.6 Areas of 2D cell dispersion over Matrigel™-, laminin-, and TBS-coated scaffolds at 0, 3, 5, and 7 days post-seeding. Data points are expressed as a multiple of the initially-seeded (T=0). Areas are shown as means and standard deviations (shown via error bars) (N=4 at every time point for Matrigel™- and laminin-coated scaffolds; N=2 at every time point for TBS-coated scaffolds).

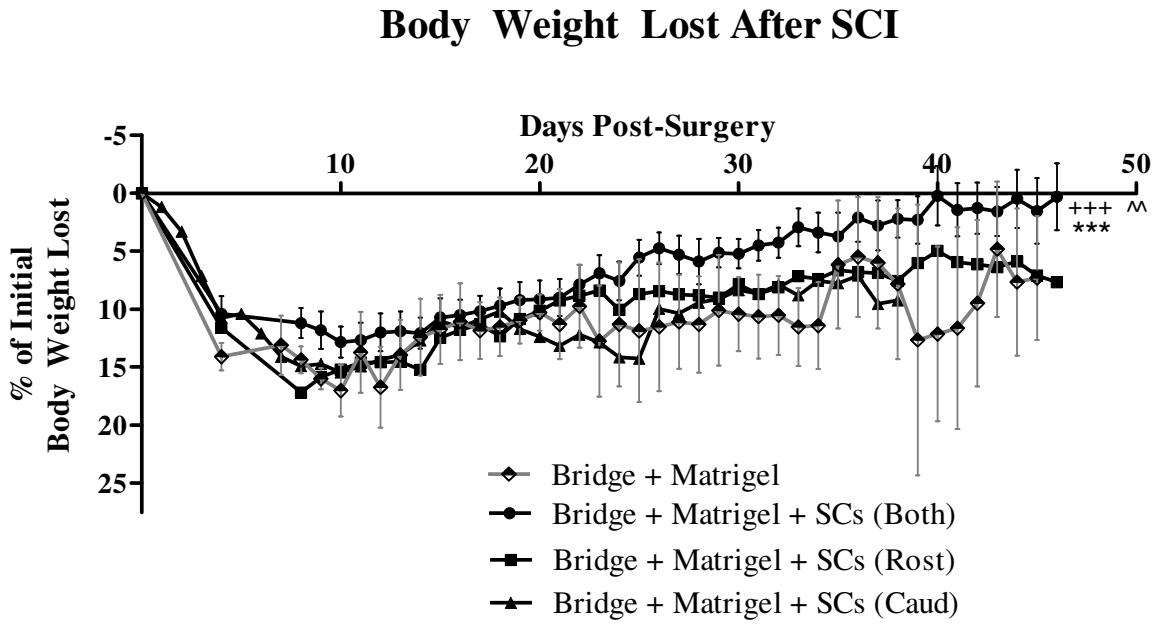
Body Weight Lost After SCI
Days Post-Surgery
-5
0
5
10
15
20
25
10
20
30
40
50
% of Initial
Body Weight Lost
+++
***
^^
Bridge + Matrigel
Bridge + Matrigel + SCs (Both)
Bridge + Matrigel + SCs (Rost)
Bridge + Matrigel + SCs (Caud)

Figure 2.7 Graph of the percent of initial body weight lost in rats after SCI. Data points are expressed at means and standard deviations (shown via error bars) (N=4). +++ significantly different from bridge + Matrigel^{TM} + SCs (Caud), $p<0.0001$. *** significantly different from bridge + Matrigel^{TM}, $p<0.0001$. ^^ significantly different from bridge + Matrigel^{TM} + SCs (Rost), $p<0.001$.

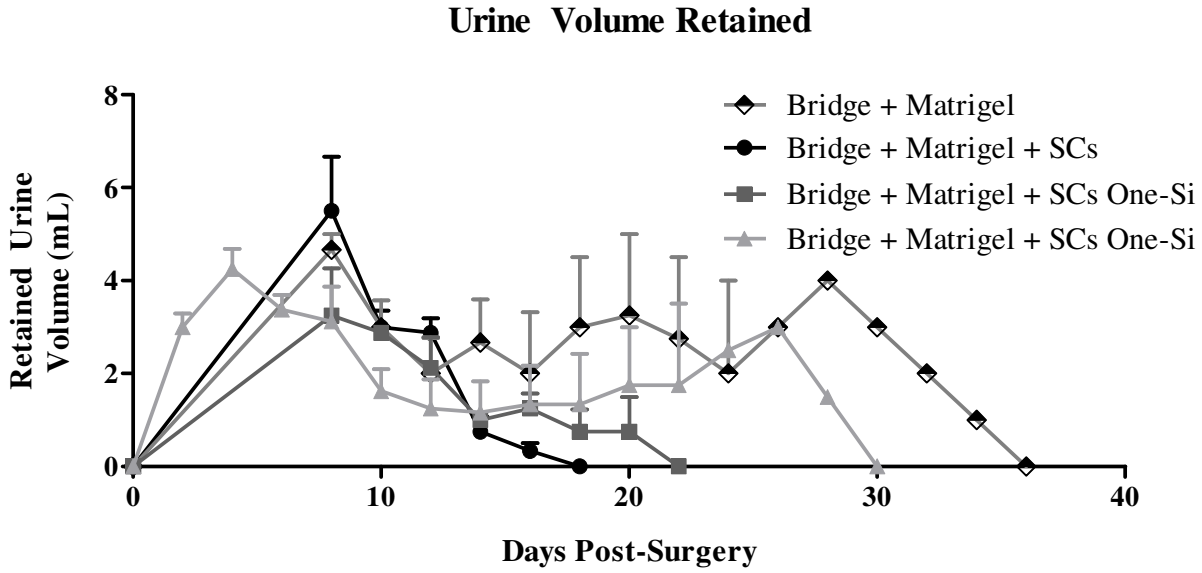
Urine Volume Retained
Retained Urine Volume (mL)
8
6
4
2
0
0
10
20
30
40
Days Post-Surgery
Bridge + Matrigel
Bridge + Matrigel + SCs
Bridge + Matrigel + SCs One-Si
Bridge + Matrigel + SCs One-Si

Fig 2.8 Graph of the amount of retained urine over time in rats after SCI. Data points are expressed as means and standard deviations (shown via error bars) (N=4). Groups means showed no significant differences. Data points without standard error of means represent only one animal.

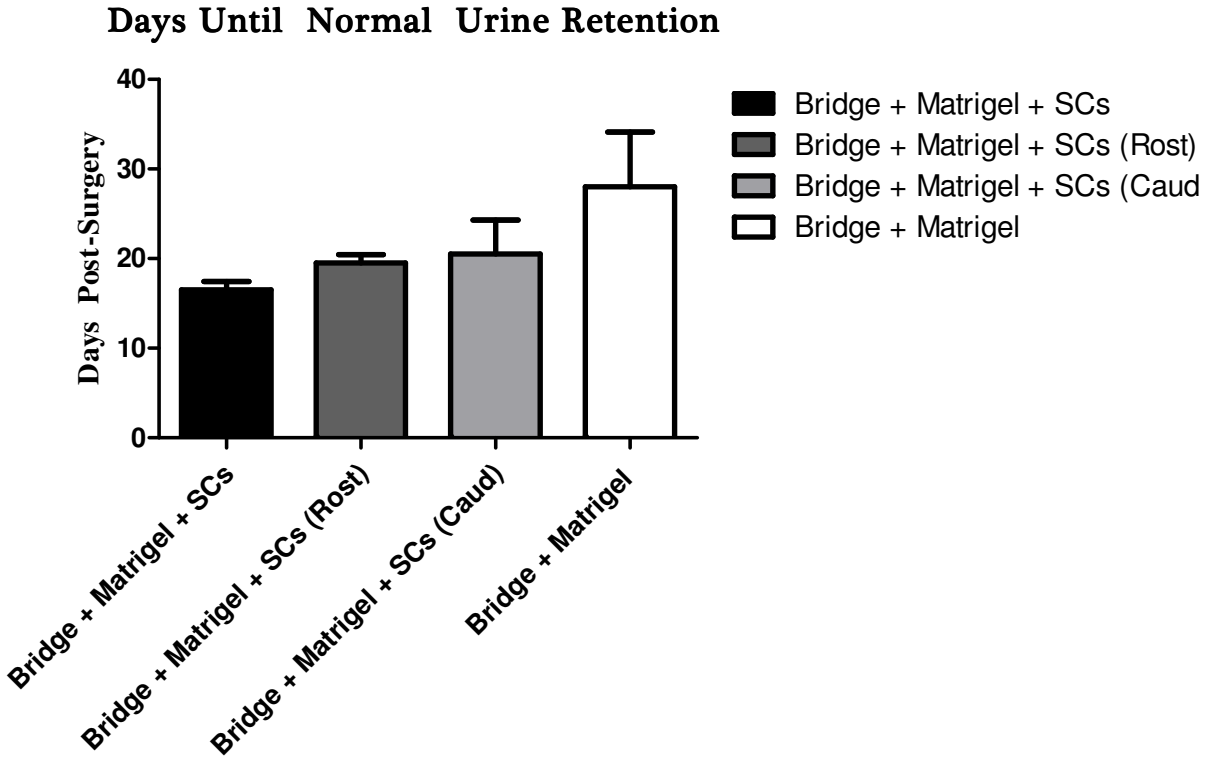
Days Until Normal Urine Retention
Days Post-Surgery
40
30
20
10
0
Bridge + Matrigel + SCs
Bridge + Matrigel + SCs (Rost)
Bridge + Matrigel + SCs (Caud)
Bridge + Matrigel
Bridge + Matrigel + SCs
Bridge + Matrigel + SCs (Rost)
Bridge + Matrigel + SCs (Caud
Bridge + Matrigel

Fig 2.9 Graph of the amount time for each treatment group to return to a state of normal urine retention . Data points are expressed as means and standard deviations (shown via error bars) (N=4). Groups means showed no significant difference.

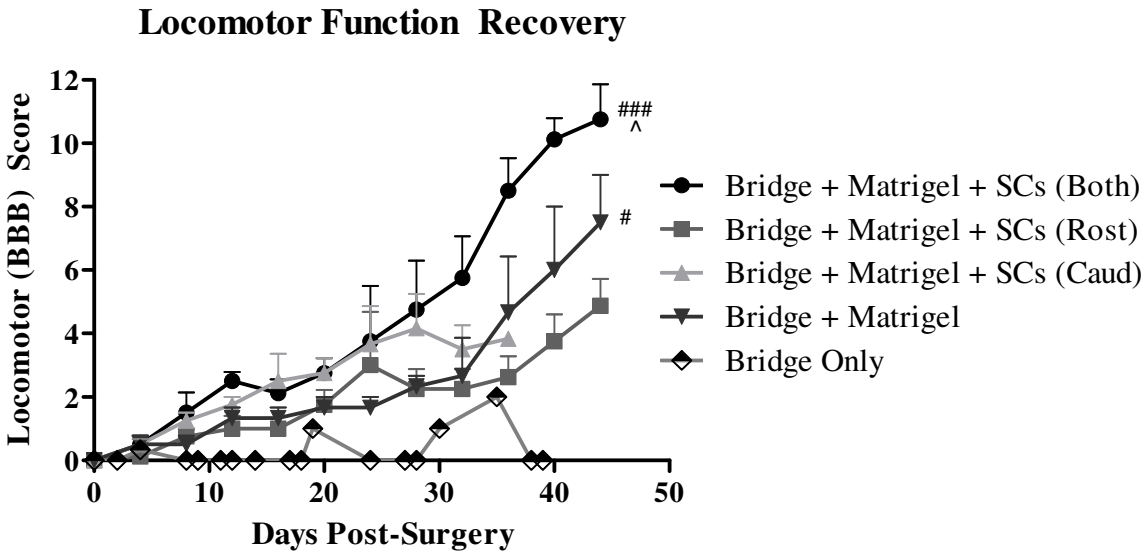
Locomotor Function Recovery
Locomotor (BBB) Score
Days Post-Surgery
0
2
4
6
8
10
12
0
10
20
30
40
50
###
^
#
Bridge + Matrigel + SCs (Both)
Bridge + Matrigel + SCs (Rost)
Bridge + Matrigel + SCs (Caud)
Bridge + Matrigel
Bridge Only

Fig 2.10 Graph of BBB locomotor scale scores over time in rats after SCI. Data points are expressed as means and standard deviations (shown via error bars) (N=4). Groups means showed no significant difference. ### significantly different from bridge only, $p<0.0001$. # significantly different bridge only, $p<0.05$. ^ significantly different from bridge + Matrigel^{TM} + SCs (Rost), $p<0.05$.

(a)

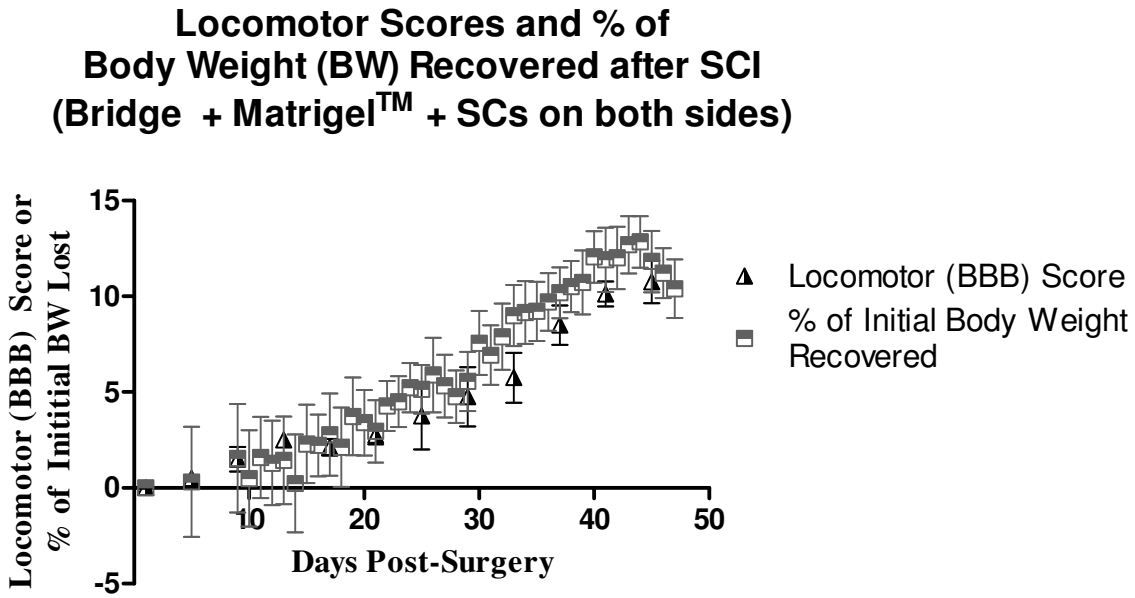
Locomotor Scores and % of
Body Weight (BW) Recovered after SCI
(Bridge + Matrigel™ + SCs on both sides)
Locomotor (BBB) Score or
% of Initial BW Lost
15
10
5
0
-5
10
20
30
40
50
Days Post-Surgery
Locomotor (BBB) Score
% of Initial Body Weight
Recovered

(b)

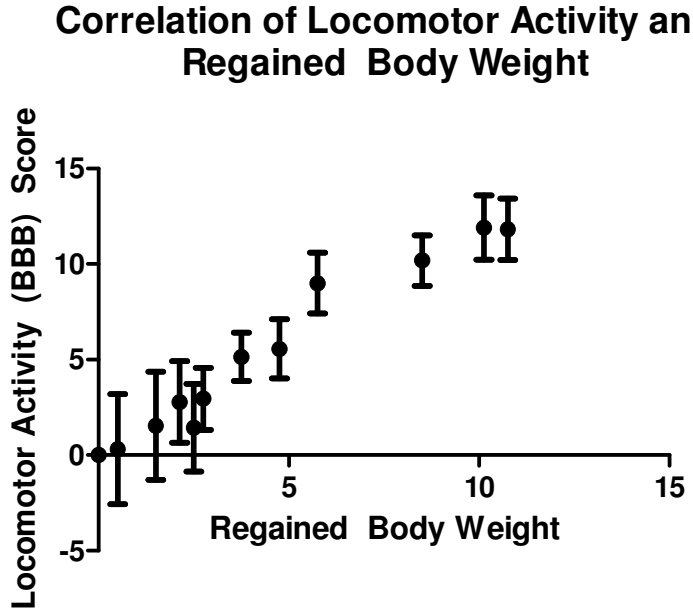
Correlation of Locomotor Activity and
Regained Body Weight
Locomotor Activity (BBB) Score
15
10
5
0
-5
5
10
15
Regained Body Weight

Fig 2.11 Graphs showing the co-variation (or correlation) between locomotor (BBB) scale score and percent of initial body weight lost for the SC bridges (both sides) treatment group. Data points are expressed as means and standard deviations (N=4) (a) BBB scores and percent of initial body weights of rats presented on the same scale and axis over time. (b) A correlational graph analysis of the two variables. BBB Score and percent of initial body weight lost were significantly correlated, $p<0.0001$.

DISCUSSION

The goals of the experiments detailed in this paper were to evaluate 3D cell migration into electrospun polydioxanone scaffolds and to improve 2D cell dispersion across the same substrate. We also aimed to improve functional recovery, as measured by the return of locomotor activity, micturition control, and body weight, in rat models of completely transected spinal cords, via the implantation of SC-seeded polydioxanone electrospun scaffolds. As noted by Kubinova & Sykova (2012), one of the more significant advantages of a complete transection model is that it allows experimenters to distinguish between true axonal regeneration and improved functional behavior due to the collateralization of intact axons.

Evaluating the Extent of 3D SC Migration

First, we characterized 3D SC migration via immunostaining and cell-counting at different depths throughout an SC-seeded scaffold. Though a substantial percent of the number of initially-seeded cells were present on the scaffold surface five days after seeding cells onto one side of 1mm-thick sliced electrospun scaffolds, markedly fewer cells were found at 250 µm, and even fewer, significantly, at 500 µm, into the scaffold. Thus, a significant amount of attached cells remained at the scaffold surface or within the first 250 µm, while a few migrated to 250 µm, and a significantly smaller portion migrated to 500 µm, arguing for the inefficacy of 3D cell migration in these experiments. Work by other groups have reported similar findings, for example, in aligned, 1 mm-thick electrospun PCL meshes, human and bovine meniscus fibrochondrocytes infiltrated, at best, two-thirds of the full 1mm distance after ten weeks (Baker et al., 2008; Baker et al., 2009). Previous studies concede that a primary limitation of electrospun scaffolds is their inability to facilitate infiltration, or 3D migration, alleging that their tightly

packed conformation of nanofibers (fibers with diameters on a nanometer scale) allow for superficial cellular growth and migration, however not for migration deep within the electrospun construct (Blakeney et al., 2011; Phipps et al., 2012; Nerurkar et al., 2011). Cell ingress into even 0.5 mm-thick nanofibrous scaffolds has been limited (Baker et al., 2009; Baker and Mauck, 2007). As pointed out by Nerurkar et al. (2011), the eventual clinical application of these constructs will likely require them to be much thicker than 1 mm, and thus limited cell infiltration poses a noteworthy challenge, especially since there are even differences between *in vitro* and *in vivo* infiltration. Other studies have approached this challenge by increasing the space between fibers, decreasing fiber diameter, or a combination of the two, altering construct porosity and offering a less spatially obstructive path for cell migration (Phipps et al., 2012; Vaquette et al., 2011).

Implications of Matrigel™ and Laminin in 2D SC Dispersion

In the current study, we approached the challenge of cell dispersion outlined above at the 2D, rather than at the 3D, level. Cell growth- and dispersion-enhancing substrates laminin and Matrigel™ were employed to first facilitate 2D dispersion, with the prospect of pursuing a similar question about migration through 3D scaffolds. Though our hypothesis that Matrigel™ would be more effective than laminin in facilitating 2D cell dispersion was not significantly supported, our data show trends that suggest that further research may yet yield results to support our hypothesis. The lack of significant difference in the mean areas covered by cells on Matrigel™-, laminin-, and TBS-coated scaffolds is consistent with reports from other similar studies (Thompson, Thomas, and Metcalfe, 1993; Hoffman, Kibbey, Letterio, and Kleinman, 1996). In fact, Matrigel™ and laminin displayed no differences from each other even when they

were independently found to be significantly more effective than other popularly studied substrates, such as fibronectin, collagen, and poly-D-lysine in supporting human embryonic stem cell (hESC) migration and differentiation (Ma et al., 2008). It is interesting, therefore, that, in the current study, Matrigel™- and laminin-coated scaffolds did not produce results that were significantly different than those produced by TBS (control)-coated scaffolds. Notably, however, a graphical trend analysis of the three groups of coated scaffolds show that, even though the difference is non-significant, TBS-coated scaffolds did not facilitate dispersion as effectively as Matrigel™- or laminin-coated scaffolds. Also, as can be seen in Figure 2.5, Matrigel™-coated scaffolds seemed to facilitate cell proliferation more effectively than laminin-coated scaffolds or TBS-coated scaffolds, resulting a cell-covered area that is markedly more dense with cells at T = 7 days than the cell-covered area of both of the other groups at the same time point.

The Improvement of Locomotor Activity

SCs vs. Matrigel™ vs. Their Combination

In our *in vivo* experiments we were able to identify between-group differences in functional locomotor activity recovery and in body weight recovery after post-surgery weight loss, but not in the restoration of control over micturition. Though a one-way ANOVA between groups for the recovery of functional locomotor activity yielded significance at the $\alpha = 0.0001$ level, a post-hoc Tukey's Multiple Comparison (Tukey's) Test revealed that only the following three comparisons had significant differences (presented as the more effective treatment vs. the less effective treatment): (1) SC bridges (both sides) vs. control bridges, (2) SC bridges (both sides) vs. rostrally-facing SC bridges, and (3) Matrigel™-only bridges vs. control bridges. Despite these significant effects of Matrigel™-only and the combination of Matrigel™ and SCs

on functional locomotor improvement, no significant differences were seen as a result of the independent action of SCs. This lack of significant difference could be attributed to the tendency of SCI treatment effects to be sub-additive (meaning when treatments are combined, the resulting effect is not a simple sum of their effects as independent treatments). Since Matrigel™ already had a significant effect in improving SCI recovery in our rat model, SCs would have had to produce a fully additive effect to that of Matrigel™ in order to appear significant in combination with Matrigel™. Thus, SCs may still have an effect that is undetectable by a statistical test like a one-way ANOVA. In fact, a two-way repeated measures ANOVA test showed that all group comparisons except for control bridge vs. caudally-facing SC bridge groups and rostrally-facing SC bridge vs Matrigel-only bridge groups differed significantly by the last time-point of 44 days. Supporting this notion, as shown in Figure 2.10, it is graphically clear that the (+)SC and (-)SC groups, when compared, are different. Specifically, the SC bridge (both sides) improved SCI recovery more than its counterpart without SCs (Matrigel™-only bridges), confirming the chance that SCs do, indeed, have an effect, albeit sub-additive and non-significant in these studies. Partially supporting the stated hypothesis as it relates to locomotor function, the combination of SCs, scaffold, and Matrigel™ produced significantly different results from the control bridge group (scaffold only), but not from the Matrigel™-only group.

Matrigel™-Coated Scaffolds Alone Produce Improved Locomotion

As hypothesized, and mentioned above, there was a marked mean difference between animals with SC bridges (both sides) and animals with control bridges. This finding supports the strongly established claim that implanted SCs, especially in the presence of Matrigel™, promote locomotive function after SCI (Bunge, 2008; Oudega, 2007; Xu et al., 1995). The significant

difference found between animals with Matrigel™-only bridges and animals with control bridges partially agrees with and partially complements findings by other groups. For example, while Tsai et al. (2006) shows that the total axon density within a synthetic hydrogel channel was significantly increased with Matrigel™, however alleged that it did not produce improvements in locmotor function. Our findings show that Matrigel™ does, indeed, improve locomotor function, supporting its wide use in the application of SCs, and other cell types, to improve SCI recovery (Fouad et al., 2005; Tsai et al., 2006; Xu et al., 1995; Xu et al., 1997). It is important to note that 2 of the 3 animals that died were of the Matrigel-only bridge group (one died at 10 days and the other at 35 days). These deaths speculate upon the inadequacy of Matrigel, in addition to electrospun bridges, to block SCI-related mortality.

Possible Error in Finding a Mean Difference Between Rostrally- vs. Caudally-Localized SCs

The significantly larger improvement in locomotor activity in SC bridge (both sides) rats, when compared to rostrally-facing SC bridge rats, but not when compared to caudally-facing SC bridge rats, is a surprising result. This suggests that caudally-facing SC bridges improve functional locomotion in rats better than their rostrally-facing counterparts. Though this may be explained anatomically, the lack of significant improvements in locomotor function in animals with either rostrally- or caudally-facing SC bridges, compared to animals treated with control bridges, suggest that this difference may be due to statistical error, possibly because of the small sample size used (N=4). Further supporting this assertion, there was also no difference in the effect on locomotor function recovery between rostrally- and caudally-facing SC bridge groups.

Trend Differences in the Urine Retention

Though there was no significant variance between groups in the retention of urine, there was a discernible trend. Additionally, the perceivable difference trend between groups in the number of days until rats yield zero retained urine volume suggests that any effect on retention becomes more apparent as treatments are combined (i.e. the number of days until normal urine retention is achieved decreases steadily from the Matrigel™-only bridge group, to the one-side seeded SC bridge groups, and finally to the SC bridge (both sides) group, which displays the shortest average time until normal urine retention is regained). Thus, the hypothesis that the combination of SCs, scaffold, and Matrigel™ will restore normal urine retention more effectively than control bridge or Matrigel™-only bridge groups may arguably, though non-significantly, be supported.

Combinatorial Approaches Effectively Occurred Alongside Body Weight Changes

The effect on body weight restoration of the combinatorial treatment of bridge + Matrigel™ + SCs on both sides (SC bridge (both sides)), when compared to body weight restoration as a result of all other groups, was significantly greater at least at the $\alpha = .001$ level, thus strongly supporting the stated hypothesis and furthermore shows the power of this combinatorial treatment. Changes in body weight may represent a more comprehensive recovery after SCI, since so many physiological factors contribute to body weight management.

Confirming the Combinatorial Treatment's Effect in on Body Weight and Locomotor Activity Restoration

Since the animals with SC bridges (both sides) showed significantly more effect, when at least compared to the bridge control group, in the restoration of body weight and locomotor activity, a correlational analysis was performed between body weight changes and locomotor function improvements in animals with SC bridges (both sides). The demonstration that these two measures are highly correlated suggests that any experimental group that displays highly significant differences from other groups in one measure should also do so in the other measure. This held true with the SC bridge (both sides) group of rats, importantly strengthening the claim of their significance, considering the small sample sizes analyzed. This significant correlation also argues for possible similar homeostatic mechanisms for locomotor control and weight management.

CONCLUSION

The current study found that 3D SC migration is highly limited and that 2D dispersion may be further facilitated by Matrigel™ or laminin. Though, the hypothesis that Matrigel™ would be more effective than laminin in facilitating 2D SC dispersion was not significantly supported. Bridges with Matrigel™ and SCs (on both sides of the scaffold) were found to be significantly better when compared to control bridges, in improving locomotor activity, and when compared to all other treatments, in restoring body weight after SCI-induced weight loss. This supports our previously stated hypothesis that the combination would be effective; only trending differences were found between groups in their effect on retained urine volumes, thus the hypothesis about the treatment combination's ability to significantly affect the restoration of micturition control was not supported . A correlational analysis further established the significance of the effects of a fully combinatorial treatment (SCs + scaffold + Matrigel™). This study showed that the particular combination of SCs, electrospun scaffold, and Matrigel™ successfully facilitated the substantial attachment of SCs to the scaffold surface. We also demonstrated that once implanted as a bridge, this combination successfully improved functional recovery, as measured by body weight restoration and improvements in locomotor activity, after SCI in rats. More work is needed to optimize 2D and 3D SC migration into scaffolds to be implanted into SCI sites, which may further improve functional recovery. However, currently available evidence suggests that SCS, interpolated throughout the SCI site on a guidance and physical support-providing scaffold, may be among the most simple, yet comprehensive, approaches to improve recovery after SCI.

REFERENCES

Afshari, F., & Fawcett, J. W. (2012). Astrocyte-Schwann-Cell Coculture Systems. In R. Milner (Ed.), *Methods in Molecular Biology: Astrocytes* (Vol. 814, pp. 381-391). Totowa, NJ: Humana Press.

Afshari, F. T., Kwok, J. C., & Fawcett, J. W. (2010). Astrocyte-produced ephrins inhibit schwann cell migration via VAV2 signaling. *The Journal of neuroscience : the official journal of the Society for Neuroscience*, *30*(12), 4246-55.

Aguayo, A. J., David, S., & Bray, G. M. (1981). Influences of the glial environment on the elongation of axons after injury: transplantation studies in adult rodents. *The Journal of experimental biology*, *95*, 231-40.

Alilain, W. J., Horn, K. P., Hu, H., Dick, T. E., & Silver, J. (2011). Functional regeneration of respiratory pathways after spinal cord injury. *Nature*, *475*(7355), 196-200. Nature Publishing Group.

Almad, A., Sahinkaya, F. R., & McTigue, D. M. (2011). Oligodendrocyte fate after spinal cord injury. *Neurotherapeutics : the Journal of the American Society for Experimental NeuroTherapeutics*, *8*(2), 262-73.

Andrews, M. R., & Stelzner, D. J. (2007). Evaluation of olfactory ensheathing and schwann cells after implantation into a dorsal injury of adult rat spinal cord. *Journal of Neurotrauma*, *24*(11), 1773-92.

Azari, M.F., Profyris, C., Karnezis, T., Bernard, C.C., Small, D.H., Cheema, S.S., Ozturk, E., Hatzinisiriou, I., Petratos, S. (2006) Leukemia inhibitory factor arrests oligodendrocyte death and demyelination in spinal cord injury. *Journal of Neuropathology and Experimental Neurology*, *65*(9), 914-929.

Baker, B. M., Gee, A. O., Metter, R. B., Nathan, A. S., Marklein, R. a, Burdick, J. a, & Mauck, R. L. (2008). The potential to improve cell infiltration in composite fiber-aligned electrospun scaffolds by the selective removal of sacrificial fibers. *Biomaterials*, *29*(15), 2348-58.

Baker, B. M., & Mauck, R. L. (2007). The effect of nanofiber alignment on the maturation of engineered meniscus constructs. *Biomaterials*, *28*(11), 1967-77.

Baker, B. M., Nathan, A. S., Huffman, G. R., & Mauck, R. L. (2009). Tissue engineering with meniscus cells derived from surgical debris. *Osteoarthritis and cartilage / OARS, Osteoarthritis Research Society*, *17*(3), 336-45.

Bao, F., Omana, V., Brown, A., Weaver, Lynne (2011). The systemic inflammatory response after spinal cord injury in the rat is decreased by alpha4 beta1 integrin blockade. *Journal of Neurotrauma*. *Epub ahead of print*.

Basso, D. M., Beattie, M. S., & Bresnahan, J. C. (1995). A sensitive and reliable locomotor rating scale for open field testing in rats. *Journal of neurotrauma*, *12*(1), 1-21.

Benton, G., Kleinman, H. K., George, J., & Arnaoutova, I. (2011). Multiple uses of basement membrane-like matrix (BME/Matrigel) in vitro and in vivo with cancer cells. *International journal of cancer. Journal international du cancer*, *128*(8), 1751-7.

Blakemore, W. F. (1975). Remyelination by Schwann cells of axons demyelinated by intraspinal injection of 6-aminonicotinamide in the rat. *Journal of neurocytology*, *4*(6), 745-57.

Blakemore, W. F. (1977). Remyelination of CNS axons by Schwann cells transplanted from the sciatic nerve. *Nature*, *266*, 68-69.

Blakeney, B. A., Tambralli, A., Anderson, J. M., Andukuri, A., Lim, D.-J., Dean, D. R., & Jun, H.-W. (2011). Cell infiltration and growth in a low density, uncompressed three-dimensional electrospun nanofibrous scaffold. *Biomaterials*, *32*(6), 1583-90.

Bueno, E. M., Laevsky, G., & Barabino, G. a. (2007). Enhancing cell seeding of scaffolds in tissue engineering through manipulation of hydrodynamic parameters. *Journal of biotechnology*, *129*(3), 516-31.

Boyce, V. S., Park, J., Gage, F. H., & Mendell, L. M. (2012). Differential effects of brain-derived neurotrophic factor and neurotrophin-3 on hindlimb function in paraplegic rats. *The European journal of neuroscience*, *35*(2), 221-32.

Bradbury, E. J., Moon, L. D. F., Popat, R. J., King, V. R., Bennett, G. S., Patel, P. N., Fawcett, J. W., et al. (2002). Chondroitinase ABC promotes functional recovery after spinal cord injury. *Nature*, *416*(6881), 636-40.

Bresnahan, J. C., Beattie, M.S., Todd, F. D., Noyes, D. H. (1987) A behavioral and anatomical analysis of spinal cord injury produced by a feedback-controlled impaction device. *Experimental Neurology*, *95*(3), 548-70.

Bunge, M. B. (2002). Bridging the transected or contused adult rat spinal cord with Schwann cell and olfactory ensheathing glia transplants. *Progress in brain research*, *137*, 275-282.

Bunge, M. B. (2008). Novel combination strategies to repair the injured mammalian spinal cord. *The Journal of Spinal Cord Medicine*, *31*(3), 262-9.

Bunge, M. B., & Pearse, D. D. (2003). Transplantation strategies to promote repair of the injured spinal cord. *Journal of rehabilitation research and development*, *40*(4 Suppl 1), 55-62.

Butzkueven, H., Emery, B., Cipriani, T., Marriott, M.P., Kilpatrick, T.J. (2006) Endogenous leukemia inhibitory factor production limits autoimmune demyelination and oligodendrocyte loss. *Glia, 53*(7), 696-703.

Chancellor, M. B., Rivas, D. A., Huang, B., Kelly, G., Salzman, S.K. (1994) Micturition patters after spinal trauma as a measure of autonomic functional recovery. *The Journal of Urology*, *151*(1), 250-4.

Chang, I. A., Oh, M.-J., Kim, M. H., Park, S.-K., Kim, B. G., & Namgung, U. (2012). Vimentin phosphorylation by Cdc2 in Schwann cell controls axon growth via β1-integrin activation. *FASEB journal: official publication of the Federation of American Societies for Experimental Biology*, 1-13.

Chen, B. K., Knight, A. M., Madigan, N. N., Gross, L., Dadsetan, M., Nesbitt, J. J., Rooney, G. E., et al. (2011). Comparison of polymer scaffolds in rat spinal cord: A step toward quantitative assessment of combinatorial approaches to spinal cord repair. *Biomaterials*, *32*(32), 8077-86.

Chen, G., Hu, Y., Wan, H., Xia, L., Li, J., Yang, F., Qu, X., Wang, S., & Wang, Z. (2002). Functional recovery following traumatic spinal cord injury mediated by a unique polymer scaffold seeded with neural stem cells and Schwann cells. *Chinese Medical Journal*, *123*(17), 2424-2431.

Chew, S. Y., Mi, R., Hoke, A., & Leong, K. W. (2008). The effect of the alignment of electrospun fibrous scaffolds on Schwann cell maturation. *Biomaterials*, *29*(6), 653-61. Cholas, R.H., Hsu, H.P., Spector, M. (2012) The reparative response to cross-linked collagen-based scaffolds in a rat spinal cord gap model. *Biomaterials*, *33*(7), 2050-2059.

Chow, W. N., Simpson, D. G., Bigbee, J. W., & Colello, R. J. (2007). Evaluating neuronal and glial growth on electrospun polarized matrices: bridging the gap in percussive spinal cord injuries. *Neuron Glia Biology*, *3*(2), 119-126.

Courtine, G., van den Brand, R., & Musienko, P. (2011). Spinal cord injury: time to move. *Lancet*, *377*(9781), 1896-8.

Davies, S. J., Shih, C.H., Noble, M., Mayer-Proschel, M., Davies, J. E., & Proschel, C. (2011). Transplantation of specific human astrocytes promotes functional recovery after spinal cord injury. *PloS One*, *6*(3), e17328.

Deng, L. X., Hu, J., Liu, N., Wang, X., Smith, G. M., Wen, X., & Xu, X. M. (2011). GDNF modifies reactive astrogliosis allowing robust axonal regeneration through Schwann cell-seeded guidance channels after spinal cord injury. *Experimental neurology*, *229*(2), 238-50.

Dewitt, D. D., Kaszuba, S. N., Thompson, D. M., & Stegemann, J. P. (2009). Collagen I-matrigel scaffolds for enhanced Schwann cell survival and control of three-dimensional cell morphology. *Tissue engineering. Part A*, *15*(10), 2785-93.

D'Hondt, F., & Everaert, K. (2011). Urinary Tract Infections in Patients with Spinal Cord Injuries. *Current infectious disease reports*.

Ding, T., Lu, W. W., Zheng, Y., Li, Z., Pan, H., & Luo, Z. (2011). Rapid repair of rat sciatic nerve injury using a nanosilver-embedded collagen scaffold coated with laminin and fibronecting. *Regenerative Medicine*, *6*(4), 437-47.

Donato, R. (2003). Intracellular and extracellular roles of S100 proteins. *Microscopy research and technique*, *60*(6), 540-51.

Du, B. L., Xiong, Y., Zeng, C. G., He, L. M., Zhang, W., Quan, D.-P., Wu, J.-L., et al. (2011). Transplantation of artificial neural construct partly improved spinal tissue repair and functional recovery in rats with spinal cord transection. *Brain research*, *1400*, 87-98.

Duncan, I. D., Aguayo, A. J., Bunge, R. P., Wood, P. M. (1981). Transplantation of rat Schwann cells grown in tissue culture into the mouse spinal cord. *Journal of the neurological sciences*, *49*(2), 241-52.

Duncan, I. D., Hammang, J. P., & Gilmore, S. A. (1988). Schwann cell myelination of the myelin deficient rat spinal cord following X-irradiation. *Glia*, *1*(3), 233-9.

Duncan, I. D., Hammang, J. P., Jackson, K. F., Wood, P. M., Bunge, R. P., & Langford, L. (1988). Transplantation of oligodendrocytes and Schwann cells into the spinal cord of the myelin-deficient rat. *Journal of neurocytology*, *17*(3), 351-60.

Engelhardt, E. M., Micol, L. a, Houis, S., Wurm, F. M., Hilborn, J., Hubbell, J. a, & Frey, P. (2011). A collagen-poly(lactic acid-co-ε-caprolactone) hybrid scaffold for bladder tissue regeneration. *Biomaterials*, *32*(16), 3969-76. Elsevier Ltd.

Erceg, S., Ronaghi, M., Oria, M., Roselló, M. G., Aragó, M. A. P., Lopez, M. G., Radojevic, I., et al. (2010). Transplanted oligodendrocytes and motoneuron progenitors generated from human embryonic stem cells promote locomotor recovery after spinal cord transection. *Stem cells (Dayton, Ohio)*, *28*(9), 1541-9.

Esteves, A. M., Squarcini, C. F. R., Lancelloti, C. L. P., Tufik, S., de Mello, M. T. (2012) Characteristics of muscle fibers in rats with limb movements during sleep after spinal cord injury. *European Neurology*, *67*, 107-15.

Evercooren, B. V., Avellana-Adalid, V., Ben Younes-Chennoufi, a, Gansmuller, a, Nait-Oumesmar, B., & Vignais, L. (1996). Cell-cell interactions during the migration of myelin-forming cells transplanted in the demyelinated spinal cord. *Glia*, *16*(2), 147-64.

Evercooren, B. V., Avellana-Adalid, V., Lachapelle, F., & Liblau, R. (1997). Schwann cell transplantation and myelin repair of the CNS. *Multiple Sclerosis*, *3*(2), 157-161.

Evercooren, B. V., Duhamel-Clerin, E., Boutry, J. M., Hauw, J. J., & Gumpel, M.

(1993). Pathways of migration of transplanted Schwann cells in the demyelinated mouse spinal cord. *Journal of neuroscience research*, *35*(4), 428-38.

Fan, L., Wang, K., Shi, Z., Die, J., Wang, C., & Dang, X. (2011). Tetramethylpyrazine protects spinal cord and reduces inflammation in a rat model of spinal cord ischemia-reperfusion injury. *Journal of vascular surgery : official publication, the Society for Vascular Surgery [and] International Society for Cardiovascular Surgery, North American Chapter*, *54*(1), 192-200.

Fawcett, J. W., & Asher, R. A. (1999). The glial scar and central nervous system repair. *Brain research bulletin*, *49*(6), 377-91.

Field-Fote, E., Ness, L. L., & Ionno, M. (2012). Vibration Elicits Involuntary, Step-Like Behavior in Individuals With Spinal Cord Injury. *Neurorehabilitation and neural repair*.

Finnerup, N. B., & Baastrup, C. (2012). Spinal Cord Injury Pain: Mechanisms and Management. *Current pain and headache reports*.

Fortun, J., Hill, C. E., & Bunge, M. B. (2009). Combinatorial strategies with Schwann cell transplantation to improve repair of the injured spinal cord. *Neuroscience letters*, *456*(3), 124-32.

Fouad, K., Schnell, L., Bunge, M. B., Schwab, M. E., Liebscher, T., & Pearse, D. D. (2005). Combining Schwann cell bridges and olfactory-ensheathing glia grafts with chondroitinase promotes locomotor recovery after complete transection of the spinal cord. *The Journal of neuroscience : the official journal of the Society for Neuroscience*, *25*(5), 1169-78.

Gale, K., Kerasidis, H., Wrathall, J. R. (1985) Spinal cord contusion in the rat: behavioral analysis of functional neurologic impairment. *Experimental Neurology*, *88*(1), 123-34.

Gary, D. S., Malone, M., Capestany, P., Houdayer, T., & McDonald, J. W. (2012). Electrical stimulation promotes the survival of oligodendrocytes in mixed cortical cultures. *Journal of neuroscience research*, *90*(1), 72-83.

Gelain, F., Panseri, S., Antonini, S., Cunha, C., Donega, M., Lowery, J., Taraballi, F., et al. (2011). Transplantation of nanostructured composite scaffolds results in the regeneration of chronically injured spinal cords, *ACS Nano*, *5*(1), 227-236.

Golden, K. L., Pearse, D. D., Blits, B., Garg, M. S., Oudega, M., Wood, P. M., & Bunge, M. B. (2007). Transduced Schwann cells promote axon growth and myelination after spinal cord injury. *Experimental neurology*, *207*(2), 203-17.

Gordon, T., Sulaiman, O., & Boyd, J. G. (2003). Experimental strategies to promote functional recovery after peripheral nerve injuries. *Journal of the peripheral nervous system : JPNS*, *8*(4), 236-50.

Göritz, C., Dias, D. O., Tomilin, N., Barbacid, M., Shupliakov, O., & Frisén, J. (2011). A pericyte origin of spinal cord scar tissue. *Science (New York, N.Y.)*, *333*(6039), 238-42.

Griffin, J., Delgado-Rivera, R., Meiners, S., & Uhrich, K. E. (2011). Salicylic acid-derived poly(anhydride-ester) electrospun fibers designed for regenerating the peripheral nervous system. *Journal of biomedical materials research. Part A*, *97*(3), 230-42.

Guest, J. D., Hiester, E. D., & Bunge, R. P. (2005). Demyelination and Schwann cell responses adjacent to injury epicenter cavities following chronic human spinal cord injury. *Experimental neurology*, *192*(2), 384-93.

Guest, J. D., Rao, a, Olson, L., Bunge, M. B., & Bunge, R. P. (1997). The ability of human Schwann cell grafts to promote regeneration in the transected nude rat spinal cord. *Experimental neurology*, *148*(2), 502-22.

Gupta, D., Venugopal, J., Prabhakaran, M. P., Dev, V. R. G., Low, S., Choon, A. T., & Ramakrishna, S. (2009). Aligned and random nanofibrous substrate for the in vitro culture of Schwann cells for neural tissue engineering. *Acta biomaterialia*, *5*(7), 2560-9.

Hadlock, T., Sundback, C., Hunter, D., Cheney, M., & Vacanti, J. P. (2000). A polymer foam conduit seeded with Schwann cells promotes guided peripheral nerve regeneration. *Tissue engineering*, *6*(2), 119-127.

Harrison B (1985) Schwann cell and oligodendrocyte remyelination in lysolecithin-induced lesions in irradiated rat spinal cord. *Journal of the neurological sciences, 67*(2), 143-159.

Hill, C. E., Moon, L. D. F., Wood, P. M., & Bunge, M. B. (2006). Labeled Schwann cell transplantation: cell loss, host Schwann cell replacement, and strategies to enhance survival. *Glia*, *53*(3), 338-43.

Hoffman, M. P., Kibbey, M. C., Letterio, J. J., & Kleinman, H. K. (1996). Role of laminin-1 and TGF-beta 3 in acinar differentiation of a human submandibular gland cell line (HSG). *Journal of cell science*, *109 (Pt 8)*(1996), 2013-21.

Hunanyan, A. S., Petrosyan, H. a, Alessi, V., & Arvanian, V. L. (2012). Repetitive spinal electromagnetic stimulation opens a window of synaptic plasticity in damaged spinal cord: role of NMDA receptors. *Journal of neurophysiology*.

Jaerve, A., Schiwy, N., Schmitz, C., & Mueller, H. W. (2011). Differential effect of aging on axon sprouting and regenerative growth in spinal cord injury. *Experimental neurology*.

Jeffries, E. M., & Wang, Y. (2011). Biomimetic micropatterned multi-channel nerve guides by templated electrospinning. *Biotechnology and bioengineering*. Epub ahead of print.

Jeong, S. R., Kwon, M. J., Lee, H. G., Joe, E. H., Lee, J. H., Kim, S. S., Suh-Kim, H., et al.

(2012). Hepatocyte growth factor reduces astrocytic scar formation and promotes axonal growth beyond glial scars after spinal cord injury. *Experimental neurology*, *233*(1), 312-22.

Jessen, K. R., & Mirsky, R. (1999). Schwann cells and their precursors emerge as major regulators of nerve development. *Trends in neurosciences*, *22*(9), 402-10.

Jha, B. S., Colello, R. J., Bowman, J. R., Sell, S. a, Lee, K. D., Bigbee, J. W., Bowlin, G. L., et al. (2011). Two pole air gap electrospinning: Fabrication of highly aligned, three-dimensional scaffolds for nerve reconstruction. *Acta biomaterialia*, *7*(1), 203-15.

Joo, N.Y., Knowles, J. C., Lee, G.-S., Kim, J.-W., Kim, H.-W., Son, Y.-J., & Hyun, J. K. (2012). Effects of phosphate glass fiber-collagen scaffolds on functional recovery of completely transected rat spinal cords. *Acta biomaterialia*, 1-11.

Jurga, M., Dainiak, M. B., Sarnowska, A., Jablonska, A., Tripathi, A., Plieva, F. M., Savina, I. N., et al. (2011). The performance of laminin-containing cryogel scaffolds in neural tissue regeneration. *Biomaterials*, *32*(13), 3423-34.

Kamada, T., Koda, M., Dezawa, M., Anahara, R., Toyama, Y., Yoshinaga, K., Hashimoto, M., et al. (2011). Transplantation of human bone marrow stromal cell-derived Schwann cells reduces cystic cavity and promotes functional recovery after contusion injury of adult rat spinal cord. *Neuropathology : official journal of the Japanese Society of Neuropathology*, *31*(1), 48-58.

Karaoz, E., Kabatas, S., Duruksu, G., Okcu, A., Subasi, C., Ay, B., Musluman, M., et al. (2012). Reduction of lesion in injured rat spinal cord and partial functional recovery of motility after bone marrow derived mesenchymal stem cell transplantation. *Turkish neurosurgery*, *22*(2), 207-17.

Keirstead, H.S., Nistor, G., Bernal, G., Totoiu, M., Cloutier, F., Sharp, K., Steward, O. (2005) Human embryonic stem cell-derived oligodendrocyte progenitor cell transplants remyelinate and restore locomotion after spinal cord injury. *Journal of Neuroscience*, *25*(19), 4694-4705.

Kim, S. M., Lee, S. K., & Lee, J. H. (2007). Peripheral nerve regeneration using a three dimensionally cultured schwann cell conduit. *The Journal of craniofacial surgery*, *18*(3), 475-88.

Kraus, A., Täger, J., Kohler, K., Manoli, T., Haerle, M., Werdin, F., Hoffmann, J., et al. (2010). Efficacy of various durations of in vitro predegeneration on the cell count and purity of rat Schwann-cell cultures. *Journal of neurotrauma*, *27*(1), 197-203.

Krick, K., Tammia, M., Martin, R., Höke, A., & Mao, H.-Q. (2011). Signaling cue presentation and cell delivery to promote nerve regeneration. *Current opinion in biotechnology*, 2-7.

Kubinova, S., & Sykova, E. (2012). Biomaterials combined with cell therapy for treatment of spinal cord injury. *Regenerative Medicine2*, *7*(2), 207-224.

Lane, M. a, Lee, K.-Z., Salazar, K., O'Steen, B. E., Bloom, D. C., Fuller, D. D., & Reier, P. J. (2011). Respiratory function following bilateral mid-cervical contusion injury in the adult rat. *Experimental neurology*.

Lavdas, A. A., Papastefanaki, F., Thomaidou, D., & Matsas, R. (2008). Schwann cell transplantation for CNS repair. *Current medicinal chemistry*, *15*(2), 151-60.

Lee, J. Y., Chung, H., Yoo, Y. S., Oh, Y. J., Oh, T. H., Park, S., & Yune, T. Y. (2010). Inhibition of apoptotic cell death by ghrelin improves functional recovery after spinal cord injury. *Endocrinology*, *151*(8), 3815-26.

Lee, M. J., Chen, C. J., Huang, W. C., Huang, M. C., Chang, W. C., Kuo, H. S., Tsai, M. J., et al. (2011). Regulation of chondroitin sulphate proteoglycan and reactive gliosis after spinal cord transection: effects of peripheral nerve graft and fibroblast growth factor 1. *Neuropathology and applied neurobiology*, *37*(6), 585-99.

Li, W. J., Laurencin, C. T., Caterson, E. J., Tuan, R. S., & Ko, F. K. (2002). Electrospun nanofibrous structure: a novel scaffold for tissue engineering. *Journal of biomedical materials research*, *60*(4), 613-21.

Li, Z., Fang, Z. Y., Xiong, L., & Huang, X. L. (2010). Spinal cord injury-induced astrocyte migration and glial scar formation: effects of magnetic stimulation frequency. *Indian journal of biochemistry & biophysics*, *47*(6), 359-63.

Li, B. C., Xu, C., Zhang, J. Y., Li, Y., & Duan, Z. X. (2012). Differing Schwann Cells and Olfactory Ensheathing Cells Behaviors, from Interacting with Astrocyte, Produce Similar Improvements in Contused Rat Spinal Cord's Motor Function. *Journal of molecular neuroscience*.

Lin, M. S., Sun, Y. Y., Chiu, W. T., Hung, C. C., Chang, C. Y., Shie, F.-S., Tsai, S.-H., et al. (2011). Curcumin attenuates the expression and secretion of RANTES after spinal cord injury in vivo and lipopolysaccharide-induced astrocyte reactivation in vitro. *Journal of neurotrauma*, *28*(7), 1259-69.

Liu, C., Shi, Z., Fan, L., Zhang, C., Wang, K., & Wang, B. (2011). Resveratrol improves neuron protection and functional recovery in rat model of spinal cord injury. *Brain research*, *1374*, 100-9.

Liu, T., Xu, J., Chan, B. P., & Chew, S. Y. (2012). Sustained release of neurotrophin-3 and chondroitinase ABC from electrospun collagen nanofiber scaffold for spinal cord injury repair. *Journal of biomedical materials research. Part A*, *100*(1), 236-42.

Lutton, C., Young, Y. W., Williams, R., Meedeniya, A. C. B., Mackay-Sim, A., & Goss, B. (2011). Combined VEGF and PDGF treatment reduces secondary degeneration after spinal cord injury. *Journal of neurotrauma*, *29*, 957-70.

Ma, W., Tavakoli, T., Derby, E., Serebryakova, Y., Rao, M. S., & Mattson, M. P. (2008). Cell-extracellular matrix interactions regulate neural differentiation of human embryonic stem cells. *BMC developmental biology*, *8*, 90.

Macaya, D., & Spector, M. (2012). Injectable hydrogel materials for spinal cord regeneration: a review. *Biomedical Materials*, *7*(1), 012001.

Mata, M., Alessi, D., & Fink, D. J. (1990). S100 is preferentially distributed in myelin-forming Schwann cells. *Journal of neurocytology*, *19*(3), 432-42.

McCreedy, D.A. & Sakiyama-Elbert, S.E. (2012) Combination therapies in the CNS: Engineering the environment. *Neuroscience Letters*. Epub ahead of print.

Mekhail, M., Almazan, G., & Tabrizian, M. (2012). Oligodendrocyte-protection and remyelination post-spinal cord injuries: A review. *Progress in neurobiology*, *96*(3), 322-39.

Mitchel, J. A., & Hoffman-Kim, D. (2011). Cellular scale anisotropic topography guides Schwann cell motility. *PloS one*, *6*(9), e24316.

Nakajima, H., Uchida, K., Guerrero, A.R., Watanabe, S., Sugita, D., Takeura, N., Yoshida, A., et al. (2012). Transplantation of mesenchymal stem cells promotes alternative pathway of macrophage activation and functional recovery after spinal cord injury. *Journal of Neurotrama*. Epub ahead of print.

Nerurkar, N. L., Sen, S., Baker, B. M., Elliott, D. M., & Mauck, R. L. (2011). Dynamic culture enhances stem cell infiltration and modulates extracellular matrix production on aligned electrospun nanofibrous scaffolds. *Acta biomaterialia*, *7*(2), 485-91.

Nessler, J. a, Moustafa-Bayoumi, M., Soto, D., Duhon, J., & Schmitt, R. (2011). Assessment of hindlimb locomotor strength in spinal cord transected rats through animal-robot contact force. *Journal of biomechanical engineering*, *133*(12), 121007.

Novikova, L.N., Lobov, S., Wiberg, M., Novikov, L.N. (2011). Efficacy of olfactory ensheathing cells to support regeneration after spinal cord injury is influenced by method of culture preparation. *Experimental Neurology*, *229*(1), 132-142.

Özgiray, E., Serarslan, Y., Öztürk, O.H., Altaş, M., Aras, M., Söğüt S., Yurtseven, T., et al. (2012). Protective effects of edaravone on experimental spinal cord injury in rats. *Pediatric Neurosurgery*. Epub ahead of print.

Onifer, S. M., Rabchevsky, A. G., & Scheff, S. W. (2007). Rat models of traumatic spinal cord injury to assess motor recovery. *ILAR journal / National Research Council, Institute of Laboratory Animal Resources*, *48*(4), 385-95.

Ormond, D. R., Peng, H., Zeman, R., Das, K., Murali, R., & Jhanwar-Uniyal, M. (2012). Recovery from spinal cord injury using naturally occurring antiinflammatory compound curcumin. *Journal of neurosurgery. Spine*, 1-7.

Oudega, M. (2007). Schwann cell and olfactory ensheathing cell implantation for repair of the contused spinal cord. *Acta physiologica (Oxford, England)*, *189*(2), 181-9.

Park, H. W., Lim, M.-J., Jung, H., Lee, S.-P., Paik, K.-S., & Chang, M.-S. (2010). Human mesenchymal stem cell-derived Schwann cell-like cells exhibit neurotrophic effects, via distinct growth factor production, in a model of spinal cord injury. *Glia*, *58*(9), 1118-32.

Park, S. S., Lee, Y. J., Lee, S.H., Lee, D., Choi, K., Kim, W.H., Kweon, O.K., et al. (2012). Functional recovery after spinal cord injury in dogs treated with a combination of Matrigel and neural-induced adipose-derived mesenchymal stem cells. *Cytotherapy*.

Patel, V., Joseph, G., Patel, A., Patel, S., Bustin, D., Mawson, D., Tuesta, L. M., et al. (2010). Suspension matrices for improved Schwann-cell survival after implantation into the injured rat spinal cord. *Journal of neurotrauma*, *27*(5), 789-801.

Pawar, K., Mueller, R., Caioni, M., Prang, P., Bogdahn, U., Kunz, W., & Weidner, N. (2011). Increasing capillary diameter and the incorporation of gelatin enhance axon outgrowth in alginate-based anisotropic hydrogels. *Acta biomaterialia*, *7*(7), 2826-34.

Pearse, D. D., Sanchez, A. R., Pereira, F. C., Andrade, C. M., Puzis, R., Pressman, Y., Golden, K., et al. (2007). Transplantation of Schwann cells and/or olfactory ensheathing glia into the contused spinal cord: Survival, migration, axon association, and functional recovery. *New York*, *1000*, 976-1000.

Phipps, M. C., Clem, W. C., Grunda, J. M., Clines, G. a, & Bellis, S. L. (2012). Increasing the pore sizes of bone-mimetic electrospun scaffolds comprised of polycaprolactone, collagen I and hydroxyapatite to enhance cell infiltration. *Biomaterials*, *33*(2), 524-34.

Plemel, J. R., Chojnacki, A., Sparling, J. S., Liu, J., Plunet, W., Duncan, G. J., Park, S. E., et al. (2011). Platelet-derived growth factor-responsive neural precursors give rise to myelinating oligodendrocytes after transplantation into the spinal cords of contused rats and dysmyelinated mice. *Glia*, *59*(12), 1891-910.

Pollard, J. D., & Armati, P. J. (2011). CIDP – the relevance of recent advances in Schwann cell / axonal neurobiology. *Journal of the Peripheral Nervous System*, *23*, 15-23.

Raisman, G. (1978). What hope for repair of the brain? *Annals of neurology*, *3*(2), 101-6.

Ritz, M. F., Graumann, U., Gutierrez, B., & Hausmann, O. (2010). Traumatic spinal cord injury alters angiogenic factors and TGF-beta1 that may affect vascular recovery. *Current neurovascular research*, *7*(4), 301-10.

Saadai, P., Nout, Y. S., Encinas, J., Wang, A., Downing, T. L., Beattie, M. S., Bresnahan, J. C., et al. (2011). Prenatal repair of myelomeningocele with aligned nanofibrous scaffolds-a pilot study in sheep. *Journal of pediatric surgery*, *46*(12), 2279-83.

Sauerbeck, A., Hunter, R., Bing, G., & Sullivan, P. G. (2011). Traumatic brain injury and trichloroethylene exposure interact and produce functional, histological, and mitochondrial deficits. *Experimental neurology*, *234*(1), 85-94.

Schaub, N. J., & Gilbert, R. J. (2011). Controlled release of 6-aminonicotinamide from aligned, electrospun fibers alters astrocyte metabolism and dorsal root ganglia neurite outgrowth. *Journal of neural engineering*, *8*(4), 046026.

Schnell, E., Klinkhammer, K., Balzer, S., Brook, G., Klee, D., Dalton, P., & Mey, J. (2007). Guidance of glial cell migration and axonal growth on electrospun nanofibers of poly-epsilon-caprolactone and a collagen/poly-epsilon-caprolactone blend. *Biomaterials*, *28*(19), 3012-25.

Selzer, M. E. (1978). Mechanisms of functional recovery and regeneration after spinal cord transection in larval sea lamprey. *The Journal of physiology*, *277*, 395-408.

Semler, J., Wellmann, K., Wirth, F., Stein, G., Angelova, S., Ashrafi, M., Schempf, G., et al. (2011). Objective measures of motor dysfunction after compression spinal cord injury in adult rats: correlations with locomotor rating scores. *Journal of neurotrauma*, *28*(7), 1247-58.

Shahin, K., & Doran, P. M. (2010). Improved seeding of chondrocytes into polyglycolic acid scaffolds using semi-static and alginate loading methods. *Biotechnology progress*, *27*(1), 191-200.

Sharma, H. S., & Sharma, A. (2012). Neurotrophic Factors. In S. D. Skaper (Ed.), *Spinal Cord* (Vol. 846, pp. 393-415). Totowa, NJ: Humana Press.

Sharp, K. G., Flanagan, L. a, Yee, K. M., & Steward, O. (2010). A re-assessment of a combinatorial treatment involving Schwann cell transplants and elevation of cyclic AMP on recovery of motor function following thoracic spinal cord injury in rats. *Experimental neurology*.

Shechter, R., Raposo, C., London, A., Sagi, I., & Schwartz, M. (2011). The Glial Scar-Monocyte Interplay: A Pivotal Resolution Phase in Spinal Cord Repair. (R. L. Mosley, Ed.)*PloS ONE*, *6*(12), e27969.

Shen, J., Fu, X., Ou, L., Zhang, M., Guan, Y., Wang, K., Che, Y., et al. (2010). Construction of ureteral grafts by seeding urothelial cells and bone marrow mesenchymal stem cells into polycaprolactone-lecithin electrospun fibers. *The International journal of artificial organs*, *33*(3), 161-70.

Shen, Y., Qian, Y., Zhang, H., Zuo, B., Lu, Z., Fan, Z., Zhang, P., et al. (2010). Guidance of olfactory ensheathing cell growth and migration on electrospun silk fibroin scaffolds. *Cell transplantation*, *19*(2), 147-57.

Shen, Z. L., Berger, a, Hierner, R., Allmeling, C., Ungewickell, E., & Walter, G. F. (2001). A Schwann cell-seeded intrinsic framework and its satisfactory biocompatibility for a bioartificial nerve graft. *Microsurgery*, *21*(1), 6-11.

Siddall, P., Xu, C. L., & Cousins, M. (1995). Allodynia following traumatic spinal cord injury in the rat.

Siebert, J. R., & Osterhout, D. J. (2011). The inhibitory effects of chondroitin sulfate proteoglycans on oligodendrocytes. *Journal of neurochemistry*, *119*(1), 176-88.

Silva, N. a, Sousa, R. a, Pires, A. O., Sousa, N., Salgado, A. J., & Reis, R. L. (2011). Interactions between Schwann and olfactory ensheathing cells with a starch/polycaprolactone scaffold aimed at spinal cord injury repair. *Journal of biomedical materials research. Part A*, 470-476.

Siriphorn, A., Chompoopong, S., & Floyd, C. L. (2010). 17β-estradiol protects Schwann cells against H2O2-induced cytotoxicity and increases transplanted Schwann cell survival in a cervical hemicontusion spinal cord injury model. *Journal of neurochemistry*, *115*(4), 864-72.

Srouji, S., Kizhner, T., Suss-Tobi, E., Livne, E., & Zussman, E. (2008). 3-D Nanofibrous electrospun multilayered construct is an alternative ECM mimicking scaffold. *Journal of materials science. Materials in medicine*, *19*(3), 1249-55.

Szentivanyi, A. L., Zernetsch, H., Menzel, H., & Glasmacher, B. (2011). A review of developments in electrospinning technology: New opportunities for the design of artificial tissue structures. *The International journal of artificial organs*, *34*(10), 986-97.

Tabesh, H., Amoabediny, G., Nik, N. S., Heydari, M., Yosefifard, M., Siadat, S. O. R., & Mottaghy, K. (2009). The role of biodegradable engineered scaffolds seeded with Schwann cells for spinal cord regeneration. *Neurochemistry international*, *54*(2), 73-83.

Takami, T., Oudega, M., Bates, M. L., Wood, P. M., Kleitman, N., & Bunge, M. B. (2002). Schwann cell but not olfactory ensheathing glia transplants improve hindlimb locomotor performance in the moderately contused adult rat thoracic spinal cord. *The Journal of neuroscience : the official journal of the Society for Neuroscience*, *22*(15), 6670-81.

Tellez, I., Cabello, A., Franch, O., Ricoy, J.R. (1987) Chromatolytic changes in the central nervous system of patients with the toxic oil syndrome. *Acta neuropathologica*, *74*(4), 354-61.

Tharion, G., Indirani, K., Durai, M., Meenakshi, M., Devasahayam, S. R., Prabhav, N. R., Solomons, C., et al. (2011). Motor recovery following olfactory ensheathing cell transplantation in rats with spinal cord injury. *Neurology India*, *59*(4), 566-72.

Thompson, H. L., Thomas, L., & Metcalfe, D. D. (1993). Murine mast cells attach to and migrate on laminin-, fibronectin-, and matrigel-coated surfaces in response to Fc epsilon RI-mediated signals. *Clinical and experimental allergy : journal of the British Society for Allergy and Clinical Immunology*, *23*(4), 270-5.

Thuret, S., Moon, L. D. F., & Gage, F. H. (2006). Therapeutic interventions after spinal cord injury. *Nature reviews. Neuroscience*, *7*(8), 628-43.

Tohda, C., & Kuboyama, T. (2011). Current and future therapeutic strategies for functional repair of spinal cord injury. *Pharmacology & therapeutics*, *132*(1), 57-71.

Tsai, E. C., Dalton, P. D., Shoichet, M. S., & Tator, C. H. (2006). Matrix inclusion within synthetic hydrogel guidance channels improves specific supraspinal and local axonal regeneration after complete spinal cord transection. *Biomaterials*, *27*(3), 519-33.

Utzschneider, D. A., Archer, D. R., Kocsis, J. D., Waxman, S. G., & Duncan, I. D. (1994). Transplantation of glial cells enhances action potential conduction of amyelinated spinal cord axons in the myelin-deficient rat. *Proceedings of the National Academy of Sciences of the United States of America*, *91*(1), 53-7.

Vaquette, C., & Cooper-White, J. J. (2011). Increasing electrospun scaffold pore size with tailored collectors for improved cell penetration. *Acta biomaterialia*, *7*(6), 2544-57.

Vargas, M. E., & Barres, B. A. (2007) Why is Wallerian degeneration in the CNS so slow? *Annual Review of Neuroscience*, *30*, 153-79.

Veeravalli, K. K., Dasari, V. R., Tsung, A. J., Dinh, D. H., Gujrati, M., Fassett, D., & Rao, J. S. (2009). Human umbilical cord blood stem cells upregulate matrix metalloproteinase-2 in rats after spinal cord injury. *Neurobiology of disease*, *36*(1), 200-12.

Walker, C. L., Walker, M. J., Liu, N.-K., Risberg, E. C., Gao, X., Chen, J., & Xu, X.-M. (2012). Systemic Bisperoxovanadium Activates Akt/mTOR, Reduces Autophagy, and Enhances Recovery following Cervical Spinal Cord Injury. (X.-J. Li, Ed.)*PloS ONE*, *7*(1), e30012.

Wang, G., Hu, X., Lin, W., Dong, C., & Wu, H. (2011). Electrospun PLGA-silk fibroin-collagen nanofibrous scaffolds for nerve tissue engineering. *In vitro cellular & developmental biology. Animal*, *47*(3), 234-40.

Wang, H. B., Mullins, M. E., Cregg, J. M., McCarthy, C. W., & Gilbert, R. J. (2010). Varying the diameter of aligned electrospun fibers alters neurite outgrowth and Schwann cell migration. *Acta biomaterialia*, *6*(8), 2970-8.

Wang, J.M., Zeng, Y.-S., Wu, J.-L., Li, Y., & Teng, Y. D. (2011). Cograft of neural stem cells and schwann cells overexpressing TrkC and neurotrophin-3 respectively after rat spinal cord transection. *Biomaterials*, 1-15.

Wang, X., Duffy, P., McGee, A. W., Hasan, O., Gould, G., Tu, N., Harel, N. Y., et al. (2011). Recovery from chronic spinal cord contusion after Nogo receptor intervention. *Annals of neurology*, *70*(5), 805-21.

Wang, Y., Me, X., Zhang, L., & Lv, G. (2011). Supplement moderate zinc as an effective treatment for spinal cord injury. *Medical hypotheses*, *77*(4), 589-90.

Wang, Y., Zhao, Z., Zhao, B., Qi, H., Peng, J., Zhang, L., Xu, W., Hu, P., & Lu, S. (2011). Biocompatibility evaluation of electrospun aligned poly(propylene carbonate) nanofibrous scaffolds with peripheral nerve tissues and cells *in vitro*. *Chinese Medical Journal, 124*(15), 2361-2366.

Ward, R. E., Huang, W., Curran, O. E., Priestley, J. V., & Michael-Titus, A. T. (2010). Docosahexaenoic acid prevents white matter damage after spinal cord injury. *Journal of neurotrauma*, *27*(10), 1769-80.

Webber, C. a, Christie, K. J., Cheng, C., Martinez, J. a, Singh, B., Singh, V., Thomas, D., et al. (2011). Schwann cells direct peripheral nerve regeneration through the Netrin-1 receptors, DCC and Unc5H2. *Glia*, *000*(May), 1-15.

Wei, Y. T., He, Y., Xu, C. L., Wang, Y., Liu, B. F., Wang, X. M., Sun, X. D., et al. (2010). Hyaluronic acid hydrogel modified with nogo-66 receptor antibody and poly-L-lysine to promote axon regrowth after spinal cord injury. *Journal of biomedical materials research. Part B, Applied biomaterials*, *95*(1), 110-7.

Wright, K. T., El Masri, W., Osman, A., Chowdhury, J., & Johnson, W. E. B. (2010). Bone Marrow for the Treatment of Spinal Cord Injury: Mechanisms and Clinical Application. *Stem cells (Dayton, Ohio)*, 169-178.

Wu, B., Sun, L., Li, P., Tian, M., Luo, Y., Ren, X. (2011). Transplantation of oligodendrocyte precursor cells improves myelination and promotes functional recovery after spinal cord injury. *Injury*. Epub ahead of print.

Xu, X. M., Chen, a, Guénard, V., Kleitman, N., & Bunge, M. B. (1997). Bridging Schwann cell transplants promote axonal regeneration from both the rostral and caudal stumps of transected adult rat spinal cord. *Journal of neurocytology*, *26*(1), 1-16.

Xu, X. M., Guénard, V., Kleitman, N., & Bunge, M. B. (1995). Axonal regeneration into

Schwann cell-seeded guidance channels grafted into transected adult rat spinal cord. *The Journal of comparative neurology*, *351*(1), 145-60.

Yamashima, T. (2004) Ca2+-dependent proteases in ischemic neuronal death: a conserved 'calpain-cathepsin cascade' from nematodes to primates. *Cell Calcium, 36*(3-4), 285-93.

Yan, M., Cheng, C., Jiang, J., Liu, Y., Gao, Y., Guo, Z., Liu, H., et al. (2009). Essential role of SRC suppressed C kinase substrates in Schwann cells adhesion, spreading and migration. *Neurochemical research*, *34*(5), 1002-10.

Yang, F., Xu, C. Y., Kotaki, M., Wang, S., & Ramakrishna, S. (2004). Characterization of neural stem cells on electrospun poly(L-lactic acid) nanofibrous scaffold. *Journal of biomaterials science. Polymer edition*, *15*(12), 1483-97.

Yezierski, R. P. (2009). Spinal cord injury pain: Spinal and supraspinal mechanisms. *Science*, *46*(1), 95-107.

Yuan, Y., Su, Z., Pu, Y., Liu, X., Chen, J., Zhu, F., Zhang, H., He, C. (2011). Ethyl pyruvate promotes spinal cord repair through ameliorating the glial microenvironment. *British Journal of Pharmacology*.

Zeng, X., Zeng, Y. S., Ma, Y. H., Lu, L. Y., Du, B. L., Zhang, W., Li, Y., et al. (2011). Bone Marrow Mesenchymal Stem Cells in a Three Dimensional Gelatin Sponge Scaffold Attenuate Inflammation, Promote Angiogenesis and Reduce Cavity Formation in Experimental Spinal Cord Injury. *Cell transplantation*. Epub ahead of print.

Zhang, G., Jin, L.-Q., Sul, J.-Y., Haydon, P. G., & Selzer, M. E. (2005). Live imaging of regenerating lamprey spinal axons. *Neurorehabilitation and neural repair*, *19*(1), 46-57.

Zhang, J., Zhao, F., Wu, G., Li, Y., & Jin, X. (2010). Functional and histological improvement of the injured spinal cord following transplantation of Schwann cells transfected with NRG1 gene. *Anatomical record (Hoboken, N.J. : 2007)*, *293*(11), 1933-46.

Zhao, T., Qi, Y., Li, Y., & Xu, K. (2011). PI3 Kinase regulation of neural regeneration and muscle hypertrophy after spinal cord injury. *Molecular biology reports*. Epub ahead of print.

Zhilai, Z., Hui, Z., Yinhai, C., Zhong, C., Shaoxiong, M., Bo, Y., & Anmin, J. (2011). Combination of NEP 1-40 infusion and bone marrow-derived neurospheres transplantation inhibit glial scar formation and promote functional recovery after rat spinal cord injury. *Neurology India*, *59*(4), 579-85.

Ziegler, M. D., Hsu, D., Takeoka, A., Zhong, H., Ramón-Cueto, A., Phelps, P. E., Roy, R. R., et al. (2011). Further evidence of olfactory ensheathing glia facilitating axonal regeneration after a complete spinal cord transection. *Experimental neurology*, *229*(1), 109-19.

Zong, S., Zeng, G., Wei, B., Xiong, C., & Zhao, Y. (2011). Beneficial Effect of Interleukin-1 Receptor Antagonist Protein on Spinal Cord Injury Recovery in the Rat. *Inflammation*.